Check for updates

ADVANCING EARTH AND SPACE SCIENCE

Water Resources Research

RESEARCH ARTICLE

10.1029/2020WR029058

Key Points:

- Thirty nine well fields show diverging patterns of isotopes and noble gases revealing different vulnerability and resilience under contaminant stress
- Multiple age tracers can constrain the age distribution of mixed water from public supply well fields using a discrete groundwater age model
- The combined age distribution of the total of 0.2 km^3 annually abstracted water for public drinking water estimates: 9% is of recent origin, 56% is of Holocene age and 35% of Pleistocene age, with the percentage of the last paleo-fraction increasing in time

Supporting Information:

Supporting Information may be found in the online version of this article.

Correspondence to:

H. P. Broers,
hans-peter.broers@tno.nl

Citation:

Broers, H. P., Sültenfuß, J., Aeschbach, W., Kersting, A., Menkovich, A., de Weert, J., & Castelijns, J. (2021). Paleoclimate signals and groundwater age distributions from 39 public water works in the Netherlands; Insights From noble gases and carbon, hydrogen and oxygen isotope tracers. *Water Resources Research*, *57*, e2020WR029058. https://doi.org/10.1029/2020WR029058

Received 22 OCT 2020
Accepted 24 JUN 2021

© 2021. The Authors.
This is an open access article under the terms of the Creative Commons Attribution-NonCommercial-NoDerivs License, which permits use and distribution in any medium, provided the original work is properly cited, the use is non-commercial and no modifications or adaptations are made.

Paleoclimate Signals and Groundwater Age Distributions From 39 Public Water Works in the Netherlands; Insights From Noble Gases and Carbon, Hydrogen and Oxygen Isotope Tracers

Hans Peter Broers[1], Jürgen Sültenfuß[2], Werner Aeschbach[3,4], Arne Kersting[3], Armin Menkovich[1], Jasperien de Weert[5], and Jeroen Castelijns[6]

[1]TNO Geological Survey of the Netherlands, Utrecht, The Netherlands, [2]Department of Oceanography, Universität Bremen, Institute of Environmental Physics, Bremen, Germany, [3]Institute of Environmental Physics, Heidelberg University, Heidelberg, Germany, [4]Heidelberg Center for the Environment, Heidelberg University, Heidelberg, Germany, [5]Deltares, Utrecht, The Netherlands, [6]Brabant Water N.V., 's-Hertogenbosch, The Netherlands

Abstract Knowing the age distribution of water abstracted from public water supply wells helps to ensure customer trust in drinking water sources and underpin predictions of water quality evolution. We sampled the mixed water of 39 large public supply well fields for major ion chemistry, ^{3}H, ^{3}He, ^{18}O, ^{2}H, $^{14}C_{DIC}$, $^{13}C_{DIC}$ and noble gases and determined the Noble Gas Temperature (NGT). We used a discrete travel time distribution model to quantify the age distributions using ^{3}H, ^{4}He, ^{14}C apparent age and NGT as the 4 distinctive tracers. Helium-4 and NGT provided information on the older part of the age distributions and showed that the ^{14}C apparent ages are often the result of mixing of waters ranging between 2,000 and 35,000 years old, instead of being discrete ages with a limited variance as previously assumed. The results reveal a large range of age distributions, comprising vulnerable well fields with >60% young water (<100 years) and well fields with >30% paleo groundwater (>25,000 years) and all forms of intermediate distributions. The age distributions match the hydrogeological setting; well fields with age distributions skewed towards older ages appear in the Roer Valley Graben structure, where fluvial and marine aquitards and sealed faults provide protection from recent recharge. Waters from this graben exhibit paleoclimate signals, with a clear relation between NGT (range 3.2–9.3 °C), ^{4}He (up to 3.3×10^{-6} ccSTP/g) and $\delta^{18}O$ (range −8.5‰ to −5.9‰$_{VSMOW}$). Moreover, $^{3}He/^{4}He$ ratios of these graben waters suggest a certain influx of He from mantle origin.

1. Introduction

Worldwide, groundwater is one of the most important sources for fresh water supply. Approximately 70% of the Dutch population relies on groundwater for their drinking water, especially in the southern and eastern parts of the Netherlands where unconsolidated sandy deposits provide the best aquifers. Globally, groundwater resources are under pressure from overexploitation (Aeschbach-Hertig & Gleeson, 2012; Gleeson et al., 2012) and point and diffuse sources of pollution, especially by pesticides and nutrients from intensive use of agricultural lands. (Hansen et al., 2010; Nolan et al., 1997; Visser et al., 2007). The Netherlands is one of the most densely populated countries with an economy that is partly based on its agricultural sector. These two factors lead to high water demands and pressures on the groundwater system. The strong increase of intensive livestock farming in the Netherlands has created an increasing pressure on the groundwater pumped for drinking water supply (Mendizabal & Stuyfzand, 2011, Mendizabal et al., 2012). Although European legislation (EU, 2006) aims at reducing the leaching of agricultural contaminants to groundwater and surface water resources, many well fields for public water supply are still under threat. This resulted in the systematic closure of shallow well fields during the past 3 decades. Blending of water from different aquifers and different locations is often required to satisfy drinking water standards (e.g., Visser et al., 2013). Moreover, new developments put pressure on the available groundwater resources, such as the exponential increase of aquifer thermal energy systems in urbanized areas (Bonte et al., 2011) and the increased demands for irrigation from groundwater due to water scarcity during dry summers in agricultural areas.

Therefore, drinking water supply companies need to assess the vulnerability of their well fields and the projected water quality evolution with time in order to make decisions on expansion or replacement of well fields. The vulnerability of well fields strongly depends on the travel times of water and contaminants towards the pumping wells. The age distribution or travel time distribution is one of the key aspects to be addressed (Broers & Van Geer, 2005; Broers et al., 2004; Duffy & Lee, 1992; Etcheverry & Perrochet, 2000; Kaandorp et al., 2018; Laier, 2014; Manning et al., 2005; Osenbrück et al., 2006; Eberts et al., 2012; Visser et al., 2013). Other factors that determine the vulnerability of a well field are the history of leaching of contaminants into the groundwater (Böhlke, 2002; Broers & Van der Grift, 2004; Visser, Dubus et al., 2009; Visser et al., 2013) and the geochemical reactivity of the subsurface sediments to attenuate or adsorb nutrients and pesticides (Green et al., 2010; Landon et al., 2011; Zhang et al., 2009).

Production wells typically draw water horizontally from the aquifer layer where the filter screens are situated, but also from the aquifers and aquitards above and below, depending on the hydrogeological structure and on the amount of flow generated by pumping relative to the aquifer thickness, transmissivities and recharge rates (e.g., Bakker & Hemker, 2002; Eberts et al., 2012; Zinn & Konikow, 2007; Visser et al., 2013). Production wells therefore mix water from different depths and ages, which implies that the ages typically follow a distribution which is determined by these mixing processes. Broers and Van Geer (2005) showed that the groundwater age distribution corresponds to an exponential groundwater age distribution model for a simple case of a homogeneous unconfined aquifer with a fully penetrating pumping well, but even for a partially penetrating well with sufficient flow to capture water from the entire thickness of the aquifer. For such a simple case, the age distribution is completely determined by the logarithmic age stratification according to Vogel (1967). For our complex case, where water is potentially drawn from a number of aquifers and a range of depths in a complicated study area, such a simple model is poorly suited and the statistical model of Visser et al. (2013) is preferably used as it does not make a priori assumptions on the shape of the distributions. Visser et al. tested different types of age distributions for the large production well field Holten that is configured with multiple wells at multiple depths. Their results showed that the total Holten well field acts as a single pumped production well for which the age distribution can be described by an exponential distribution that is consistent with the logarithmic age profile in the aquifer. However, they discovered that individual pumping wells within the well field influenced each other by competing for capture area. As a result, individual well-specific age distributions are not identical to one another. Typically, deeper wells tend to rather draw the older water and shallower wells the younger water, especially if deep and shallow wells are located in close proximity (Visser et al., 2013). Visser et al. showed that it is in principle possible to derive age distributions for a pumped well with mixed water, using a suite of tracers that in total cover the complete distribution of ages, following the conceptual approaches suggested by Corcho Alvarado et al. (2007), Plummer et al., (2001) and Sültenfuß et al. (2011). In this paper, we expand the multi-tracer approach towards mixtures of water from complete well fields by analyzing multi-tracer concentrations from mixed water collected from a number of pumping wells at large water supply well fields before it is treated to become tap water. Conceptually, the method tested here is similar to analyzing multiple tracers from a single well with mixed water from different depths and ages as done for Holten (Visser et al., 2013). We hypothesize that the flow velocities generated by the pumping wells of the public supply well fields are large enough to draw water from the complete aquifer in which the wells are situated and probably also large enough to draw water from aquifers and leaky aquitards above and below the pumped aquifer. This hypothesis seems reasonable, given that the Netherlands has a centralized drinking water supply system and tap water is derived from a limited number of larger well fields, typically pumping 2×10^6 to 8×10^6 m^3/yr. These well fields typically have been operating for decades; thus we assume that a stable stationary age distribution has been reached (Zinn & Konikow, 2007).

In this study we aim to characterize and compare the tracer patterns of stable and radioactive isotopes and noble gas concentrations of all branches of the main 39 public supply well fields (a) to identify supra-regional spatial and depth patterns of waters with different recharge history that are abstracted, (b) to derive the age distributions of the 39 well fields as these are constrained by the measured tracers, (c) to assess patterns of major groundwater chemistry in relation to the age distribution of the water, and (d) to interpret the observed patterns and age distributions according to the hydrogeological setup of the area, including the faults and aquitard structures that may have defined paleo groundwater flow. We hypothesize that an age histogram approach such as the Discrete Travel Time Distribution Model (DTTDM, Visser et al., 2013)

can effectively constrain the age distributions of waters that are mixed due to the pumping itself. We aim to compare the age distributions between different well fields in order to optimize a strategy for the sustainable use of groundwater at the supra-regional scale. Eventually, this allows us to evaluate the vulnerability of these fields in relation to contaminants recharging at the surface, to assess how well protected they are and to find out whether further protection of catchment areas would be sensible and cost-effective.

2. Material and Methods

2.1. Study Area and Hydrogeological Setting

We analyzed a selection of 39 water branches of 34 public water supply well fields in the province of Noord-Brabant in the southern part of the Netherlands. The province of Noord-Brabant covers about 5,000 km^2 and is home to approximately 2.5 million inhabitants, 5.0 million pigs, 27 million poultry and 650,000 cattle. These figures show that Noord-Brabant is one of the areas in Europe with substantial environmental impacts from intensive livestock farming and urban living. As a result, leaching of diffuse pollutants to the shallow groundwater is common, although the increasing trend in leaching of agricultural inputs has been reversed due to national and Europe-wide legislation (Broers & Van der Grift, 2004; Visser et al., 2009).

Noord-Brabant is a relatively flat area with altitudes ranging from mean sea level (MSL) in the north and west to 30 m above MSL in the southeast. Phreatic water tables are generally shallow, usually within 1–5 m below the surface. Geologically, Noord-Brabant should be divided in 3 main zones, with a different hydrogeological buildup; the western part, the Roer Valley Graben in the center and the uplifted Peel Block in the east (Figure 1). The most striking geological structure is the Roer Valley Graben, a tectonic structure that has a NW-SE orientation (e.g., Houtgast & van Balen, 2000; Geluk et al., 1995; Verbeek et al., 2002; Bense, Van Balen, & De Vries, 2003). This Cenozoic rift structure is part of an old rift system that stretches from the Rhone Valley in France, through the Rhine Valley Graben in Germany, through the Roer Valley Rift System into the North Sea basin. A particular thick sequence of Tertiary and Quaternary sediments exists in the Roer Valley Graben, which thereby accommodates a large resource of fresh groundwater, estimated to a maximum thickness of 500–750 m (Houtgast and van Balen 2000; Luijendijk, ter Voorde, et al., 2011; Luijendijk, 2012). The easternmost part of the province includes the Peel Block which is uplifted relative to the Graben and supports a phreatic aquifer with a thickness of 50 meters at maximum. In the western part of Noord-Brabant the total thickness of aquifers supporting fresh groundwater is around 100–200 meters.

The hydrogeological base of the active fresh groundwater system in the Roer Valley Graben is formed by the Miocene/Early Pliocene Breda Formation that is composed of a series of perimarine, glauconite-rich clay and sand deposits. The overlying perimarine Pliocene Oosterhout (OO) and Early Pleistocene Maassluis Formations (MS) have higher transmissivity and highly conductive strata that support groundwater abstraction mainly in the western part of the study area. The main aquifers for groundwater abstraction in the Roer Valley Graben are the fluvial and estuarine gravel and sand deposits of the Rhine-Meuse system which form the bulk of the Pliocene Kieseloolite (KI) and Late Pliocene/Early Pleistocene Waalre (WA) Formations, which reach a total thickness of 300 m in the Graben. Several clay layers act as aquitards within those deposits, and especially the upper part of the Waalre Formation forms a major aquitard that confines the deeper groundwater resources below it. The Waalre deposits are partly overlain by periglacial and fluvial deposits of local rivers that drained the northern and central part of present-day Belgium, which are included in the Early Pleistocene Stramproy Formation (SY). Coarse fluvial sands and gravels of the Rhine-Meuse river system form the Middle Pleistocene Sterksel Formation (ST) which presents the main shallow aquifer in the Graben and the area immediately west of it. Further to the west these deposits were never formed, and the prime aquifers are made up of the sediments of the older Waalre and Stramproy Formations and the underlying Maassluis and Oosterhout Formations. On the eastern Peel Block, the Miocene Breda Formation was uplifted and the thin aquifers are made up of remnants from the Kieseloolite Formation and the gravels from the Meuse river that are distinguished as the Beegden Formation.

Groundwater for public water supply is abstracted from this complicated hydrogeological system at 34 centralized locations, often consisting of multiple individual pumping wells in a well field configuration of approximately 0.5 km^2. The individual pumping wells feed their water into a collective system that contains

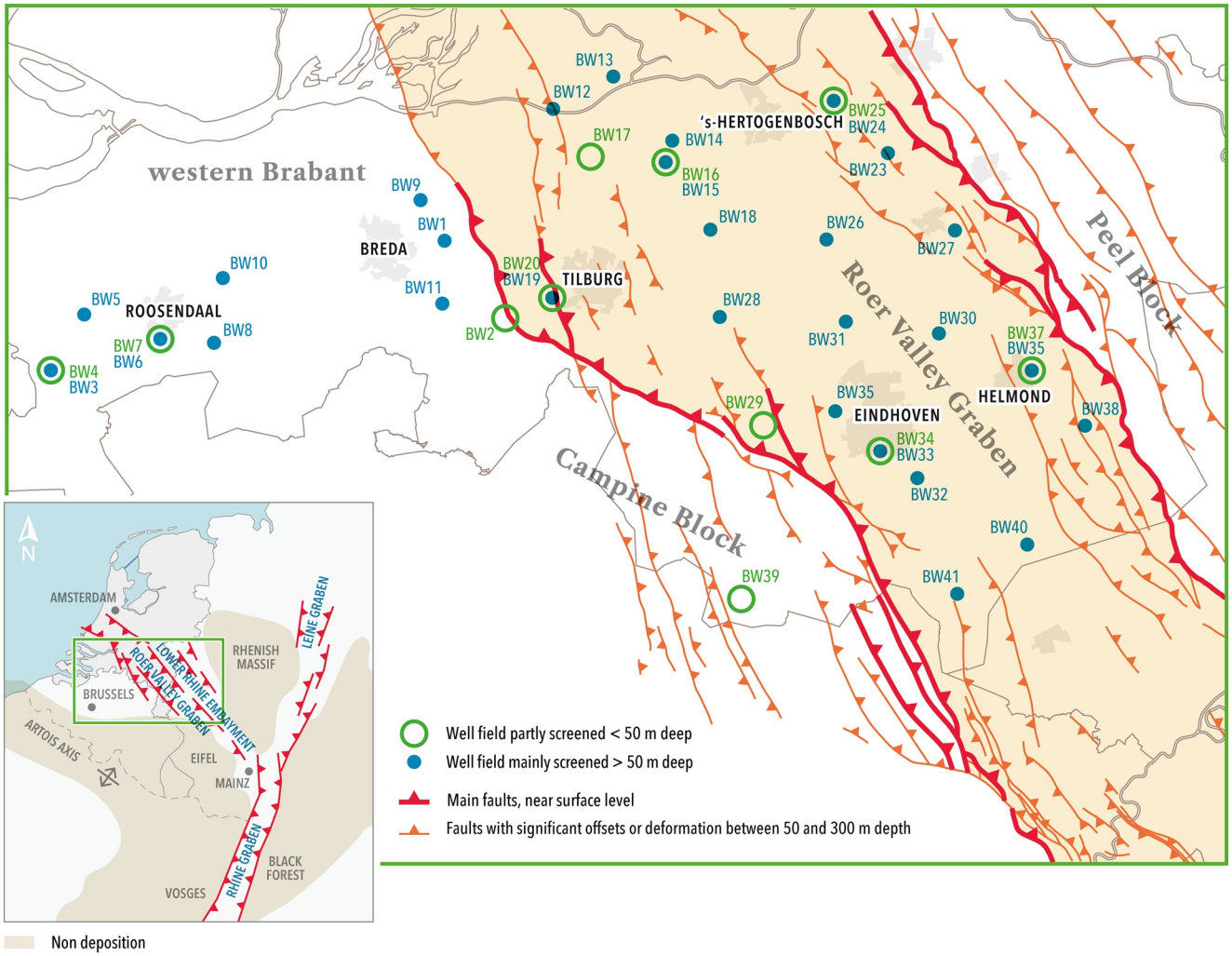

Figure 1. (a) Map of the study area in the larger European setting; The Roer Valley Graben as a connection between the Rhine Valley Graben structure and the West Netherlands Basin (after Verbeek et al., 2002) (b) Location and depth of the sampled well fields.

a collective tap point for sampling. Such a collective system of multiple pumping wells is called a "water branch," and often water branches from deeper and shallower pumps are kept separate in order to prevent clogging of the system. Public water supply in this case also includes the supply towards the farms with intensive livestock farming, which is a major user in our study area. Domestic, private wells for drinking water are almost non-existent in the area because all households are connected to the public water system. The water company Brabant Water N.V. abstracts water at these 34 centralized locations and delivers 1.80×10^8 m^3 annually. At 13 of these locations, water is abstracted from an average depth of <100 m below MSL. At the other locations water is abstracted from aquifers deeper than 100 m below MSL, up to a maximum depth of 308 m below MSL (see Supporting Information Table S1). During the last 30 years a gradual shift occurred from pumping at relatively shallow depths above 100 m depth over the whole province, towards pumping at larger depth from the deeper Roer Valley Graben aquifers.

The shallow groundwater system is recharged by surplus precipitation, but the recharge routes to the deeper parts of the Graben are relatively unknown. Groundwater flow in the aquifers between the main aquitards in the Graben is directed towards the Northwest, suggesting recharge in the SE of the Graben structure where the aquitards are less developed, but recharge may also come through diffuse flow through the confining layer or from permeable zones along the fault systems that border the Graben. The Graben is bordered by a system of faults, of which the Feldbiss and Gilze Rijen Faults form the southern and western margin (Bense, Van Balen, & De Vries, 2003; Houtgast & van Balen, 2000) and the Peel Boundary Fault system forms the

easterly border. The Feldbiss Fault zone is generally considered to be permeable to groundwater flow and has no strong indications for hydraulic head gradients that are associated with reduced conductivity of the fault zone itself. Contrary, significant horizontal head gradients are known to exist in the eastern part of the rift system, yielding evidence for sealing of the Peel Boundary Fault Zone at shallow to intermediate depth levels. Part of the evidence also comes from the existence of so-called "wijstgronden," areas where convergence of seepage of groundwater occurs along the uplifted side of the fault, indicating a low conductivity barrier at the fault zone (e.g., Bonte et al., 2013; Lapperre et al., 2019).

2.2. Well Selection, Sampling and Measurements

Samples from a number of 39 "water branches" from the operational 34 pumping stations of Brabant Water were collected between January 23 and March 13, 2014. A water branch is here defined as the collective tap point for all water that pumped from a set of individual pumping wells (See Figure S1) which draw water in a systematic, pre-defined order. For the study, a fixed number of individual pumping wells were selected to pump for at least 24 h before the sampling at the collective tap point of the water branch was done to acquire a mix of groundwater that is representative for the average pumping regime. Two samples were taken at a pumping station when water was pumped from distinct aquifers that were separated by important aquitards; one for the shallower aquifer pumped, and one for the deeper aquifer. Shallow and deep branches were sampled separately for seven well fields. Water in the collection system of the water production facility is routinely kept under pressure to avoid oxygen intrusion and subsequent clogging of the water system, which also prevents degassing. As such, samples can be considered to be undisturbed by degassing or chemical reactions that would change gas concentrations or noble gas ratios. Details about the analysis of water chemistry, isotopes and noble gases is presented in the Supporting Information Text S1.

2.3. Analyzing Patterns of Major Chemistry, Radioactive Isotopes and Noble Gases

The ages of groundwater in the upper 25 m of the subsurface are well characterized and point to groundwater that predominantly has infiltrated during the last 60 years (Visser, Dubus, et al., 2009; Visser, Broers, et al., 2009). Previous studies in this part of the Netherlands show ^{14}C activities ranging from 1 to 80 pmC in deeper parts of our study area, indicating that we may expect both young and almost ^{14}C-dead Pleistocene waters in the aquifers which are pumped for water supply (e.g., Glasbergen, 1987). Based on the expected broad range of ages we opted for the following suite of tracers: tritium (^{3}H) (Poreda et al., 1988; Schlosser et al., 1988), ^{14}C (Plummer et al., 2001), ^{4}He (Blaser, Coetsiers, et al., 2010; Gardner et al., 2011; Solomon et al., 1996; Wei et al., 2015), $^{18}O/^{2}H$ (e.g., Sukhija et al., 1998; Kralik et al., 2014; Houben et al., 2014) and the noble gases He, Ne, Ar, Kr, and Xe which enable the calculation of the Noble Gas Temperature (NGT; Aeschbach-Hertig & Solomon, 2013; Aeschbach-Hertig et al., 2000). The patterns of measured concentrations of major chemistry (Ca, Mg, Na, Cl, alkalinity), stable and radioactive isotopes (^{18}O, ^{3}H and $^{14}C_{DIC}$) and the noble gas concentrations were analyzed to interpret the data and determining processes qualitatively in terms of the age range of the mixed samples. Concentration of helium isotopes and neon were measured at the Bremen lab (Sültenfuß et al., 2009). All noble gas concentrations were analyzed at the Heidelberg lab. This enables the comparison of the measured He and Ne concentrations and computation of the radiogenic ^{4}He fraction. Inverse modeling and parameter estimation techniques were used to interpret the measured noble gases concentrations and their uncertainties, using the optimization approach described in Aeschbach-Hertig et al. (1999) and Ballentine and Hall (1999). This approach minimizes the uncertainty-weighted squared deviations between modeled and measured noble gas concentrations denoted by χ^2 (Equation 1) in order to obtain the amount of entrapped or dissolved air and the NGT.

$$\chi^2 = \sum_i \frac{\left(C_{i,o} - C_{i,m}\right)^2}{\sigma_i^2} \left(i = \text{Ne, Ar, Kr, Xe}\right) \tag{1}$$

where $C_{i,m}$ are the modeled noble gas concentrations, $C_{i,o}$ and σ^2_i are the observed noble gas concentrations and their uncertainties. Typically, groundwater exhibits concentrations of dissolved conservative atmospheric gases that exceed the atmospheric equilibrium values, a phenomenon which is denoted as "excess air." Different excess air models were conceptualized in the previous decade. Aeschbach-Hertig

and Solomon (2013) provide a recent overview. In order to ensure that all data was treated equally and to avoid artificial offsets due to the use of different excess air models within one study (Aeschbach-Hertig & Solomon, 2013; Sun et al., 2010), we adopted the Closed-system Equilibration (CE) excess air model for all samples (Aeschbach-Hertig et al., 1999). This includes three samples that showed signs of slight degassing (BW4, BW5, and BW17), indicated by negative values of the relative Ne excess ΔNe (e.g., Houben et al., 2014). For these 3 samples the CE-model was applied using the degassing case with a fractionation factor $F > 1$ (Aeschbach-Hertig et al., 2008; Aeschbach-Hertig & Solomon, 2013) yielding a possibly less reliable NGT relative to samples with excess air.

Noble Gas Temperatures were derived from the Heidelberg data set using the parameter estimation software PANGA (Jung & Aeschbach, 2018). The latest version of this program (Negele, 2020) includes the new high-precision noble gas solubility data of Jenkins et al. (2019), which leads to systematically slightly higher derived NGTs and lower ΔNe values compared to evaluations based on older solubility data. For estimating NGTs, we assumed that the recharge altitude was 10 meter above sea level, which seems appropriate for the Dutch lowland setting. Based on measured electrical conductivities in the groundwater samples we accounted for their small salinities ranging mostly between 0.2 and 0.6 g/kg. Insufficient fits were identified using a χ^2 test with a cut-off probability $P < 0.01$ for a value equal to or larger than the modeled χ^2 value. Only three samples (BW5, BW30, BW36) did not fulfill this criterion, but given their moderate χ^2 values and reasonable fit results, their NGTs were retained in the analysis nonetheless. The NGT uncertainties derived from the covariance matrix calculated in the fit procedure were in the order of 0.3–0.7 °C (Table S2). The three degassed samples (BW4, BW5, and BW17) exhibited high values of the excess air parameter A and the NGT error. In these cases, Monte Carlo simulations were used to obtain a more realistic uncertainty estimate and slightly adjusted NGTs, according to methods outlined by Jung et al. (2013).

The optimization approach also allowed us to distinguish the atmospheric and non-atmospheric sources of helium in the groundwater, considering the excess air components inherently, and thereby yields an estimate of the $^4He_{rad}$ concentration and its uncertainty. Radiogenic helium concentrations measured in groundwater can be applied as a qualitative tracer to determine groundwater residence times, as there are two major subsurface sources of helium: (a) in-situ production within the aquifer matrix by decay of U/Th and (b) inflow from the deeper subsurface or the underlying crust or mantle. The ratio of ^3He over ^4He measured in Bremen was used to evaluate the origin of the non-atmospheric helium, because helium from mantle origin and active tectonic regions is typically enriched in ^3He relative to helium originating from radioactive decay (e.g., Hilton, 2007; Banerjee et al., 2011). Well field $^3He/^4He$ ratios, plotted as R/R_A, for the individual samples were derived graphically by plotting a linear line between the atmospheric $^3He/^4He$ ratio (R_A) in a plot of Ne/He versus the ratio of $^3He/^4He$ and reading the Y-intercept value at Ne/He = 0.0.

Being aware that the samples represent a range of groundwater ages due to mixing, we denote our ^{14}C ages as being the ^{14}C apparent age of the mixture. Because different parts of the mixture may have experienced different processes with different fractionation and uptake of dead carbon, the ^{14}C apparent ages are by no means absolute indications of age of the water. For establishing ^{14}C apparent ages, the concept summarized by Han and Plummer (2016) was applied. This concept uses the isotopes of Dissolved Inorganic Carbon ($\delta^{13}C_{DIC}$ values and $^{14}C_{DIC}$ activities) in a single-sample model estimating the initial ^{14}C concentration of CO_2 ($^{14}C_0$) before dilution with dead carbon sources, following:

$$T = -\frac{5730}{ln2}\ln\left[\frac{C^{14}_{DIC}}{C^{14}_0}\right]$$

For estimating the initial $^{14}C_0$ and $\delta^{13}C_0$, we assumed that carbonate dissolution took place under closed system conditions in the deeper Brabant subsurface, and considered inputs from extra carbon from CO_2 that was produced during methanogenesis and the corresponding fractionation of ^{13}C during that process. For the process of methanogenesis we assumed a fractionation of +60‰ for the $\delta^{13}C_{DIC}$ of the produced CO_2. This is consistent with a corresponding fractionation of −60‰ for the produced methane, which resembles known $\delta^{13}C_{CH4}$ values of −80‰ to −90‰ as observed in the Noord-Brabant study region (Broers & de Weert, 2015). Different scenarios for determining $^{14}C_0$ and $\delta^{13}C_0$ were tested, yielding a range of possible

^{14}C apparent ages for each of the well fields, which were used as uncertainty bands in the DTTDM model. Details about the estimation of the ^{14}C apparent ages and the assumptions made are given in the Supporting Information Section S2. We mimic the mixing of waters with different ^{14}C apparent ages in our DTTDM model, using the ^{14}C apparent age as one of four end members of the groundwater age distribution (see Section 2.4).

2.4. Assessing Age Distributions Using the Discrete Travel Time Distribution Model

For assessing age distributions, we applied the shape-free groundwater age model, or age histogram method, that was applied earlier to the mixed water in Holten (Massoudieh et al., 2014; Visser et al., 2013). The Discrete Travel Time Distribution Model (DTTDM) yielded sensible results in the Holten case and was able to explain the temporal changes in water composition in individual wells at that well field (Broers et al., 2012). An advantage of a shape-free model concept is that it can deal with different kind of mixing regimes, including mixing waters from two or more separated aquifers, which may in some cases lead to bimodal age distributions (McCallum et al., 2017; Visser et al., 2013). Because of the large volumes of the centralized well fields in our study, we expect water to mix from all possible directions, depths and ages, and we did not consider more generic lumped models that make assumptions about the a priori distributions, such as the Exponential model (Maloszewski and Zuber, 1993, 1998; Vogel, 1967), the Dispersion model which assumes mixing along flow paths (Jurgens et al., 2012, 2016; Maloszewski & Zuber, 1982; Massmann et al., 2009; Suckow, 2014) or the Piston flow model (Eberts et al., 2012; Zinn & Konikow, 2007). At the public drinking water supply well fields that we studied, which consist of multiple production wells pumping at different depths and locations in close proximity, the wells compete for aquifer strata and capture areas as conceptually shown by Visser et al., 2013. We hypothesize that an age histogram approach such as DTTDM can effectively constrain the age distributions of waters that are mixed due to the pumping itself, yielding a comparison between different well fields that can be used to optimize a strategy for the sustainable use of groundwater at the supra-regional scale.

In the present study, we employed 4 tracers to identify the best-fit groundwater age distributions: $^{4}He_{rad}$, ^{3}H, NGT, and ^{14}C apparent age. Although the NGTs do not directly contain information about groundwater ages, they are indicative of past recharge temperatures of which a reasonable estimate is available from paleoclimate proxies (Affolter et al., 2019; Blaser, Kipfer, et al., 2010; Corcho_Alvarado et al., 2009; Isarin et al., 1998; Marcott et al., 2013; Renssen et al., 2007; Stute & Deak, 1989; Vandenberghe et al., 2004; Varsanyi et al., 2011). We hypothesized that an estimate of historical recharge temperatures can function as a constraint in the age distribution models used for this study. Of these 4 tracers, ^{4}He and ^{3}H behave conservatively when mixing samples with different concentrations, and mixing can be considered as a linear process. We presume that NGT will behave similarly, as there is a strong correlation between NGT and Xe concentrations in the groundwater ($R^2 = 0.93$ in our study) and Xe will mix conservatively as well. We tested this assumption by mixing two synthetic samples representing exact solutions of the CE excess air model with contrasting NGTs (4 vs. 9°C) and contrasting ΔNe (30% vs. 10%). These synthetic data were modeled to closely resemble actual groundwater samples from the well fields BW23 and BW8, spanning the range of NGT and ΔNe values occurring in this study. We found the deviations of fitted NGTs of the mixed synthetic samples from linear behavior to be in the order of 0.1–0.2 °C which we consider negligible for the purpose of our study (see Supplementary Information Section S5 and Figure S6).

For including information about the ^{14}C apparent age in assessing the age distributions, we took a slightly different approach because measured ^{14}C activities cannot be used as a conservative tracer without knowing the initial conditions and processes that influence the $^{14}C_{DIC}$ activity, $^{13}C_{DIC}$ values and DIC concentrations. We circumvented the use of the ^{14}C activity as a tracer and used the "average age" as an abstract parameter in the DTTDM model, which mixes linearly as conceptualized by Goode (1996), Bethke and Johnson (2002) and others. Thus, an average age is set for each DTTDM age class (Table 1) without any further assumptions, and we mix those ages linearly when mixing the water. Subsequently, we compared tracer based ^{14}C apparent ages of the samples with the averaged ages of the 10,626 DTTDM model distributions as discussed in the next paragraph. For determining the ^{14}C apparent ages of the well field samples, we used a number of scenarios that represent the conditions and hydrogeochemical processes in the study area (see Supporting Information, Section S2).

Table 1
Average Concentrations of Tracers in the Age Classes of the DTTDM Model

	DTTDM age class				
	<100 years	100–1,000 years	1,000–10,000 years	10,000–25,000 years	>25,000 years
Tracer:					
^{3}H (TU)	7.0	0.0	0.0	0.0	0.0
average age (yrs)	50	550	5,500	17,500	37,500
NGT (°C)	10	9.3	9.8	2.2	5.0
^{4}He (ccSTP g^{-1}) shallow	2.38×10^{-9}	2.61×10^{-8}	2.52×10^{-7}	8.40×10^{-7}	1.78×10^{-6}
^{4}He (ccSTP g^{-1}) deep	7.50×10^{-10}	8.25×10^{-9}	7.96×10^{-8}	2.65×10^{-7}	5.63×10^{-7}

In principle, oxygen-18 could implicitly carry age information too (Jasechko, 2016; Mook, 2006), however, in our study it appeared that the $\delta^{18}O_{VSMOW}$ values are influenced by secondary processes, probably including evaporation from open water surfaces (see Section 3.3) which makes the tracer unsuitable for our purpose. In using the tracers to derive age distributions of the mixes, we do not intend to find the absolute fraction of water within a certain age range; we rather aim at differentiating between gross patterns of age distributions, comparing the different well fields and interpreting regional patterns from that, relating them to the hydrogeological buildup.

Based on previous local studies (Broers, 1989; Stuurman et al., 1989) we predefined 5 age classes to be evaluated using the DTTDM; <100 years, 100–1,000 years, 1,000–10,000 years, 10,000–25,000 years and > 25,000 years. We realize that these age classes are somewhat arbitrary and unrefined, but they reflect the rough temporal scale for which the 4-tracer study could perform. The age classes roughly reflect modern water, late Holocene water and early Holocene water, the era just after and during the last glaciation and the pre-glacial period before, respectively. For each of the 4 tracers, we assumed an average concentration for each of the age classes based on the input function of the tracer (Table 1). For tritium, only the first age class, representing the class 0–100 years, has measurable concentrations. The ^{3}H concentration for this first age class was based on monthly measurements of tritium in precipitation of the closest measurement stations Groningen (1970–1977) and Emmerich (1978–2014) (IAEA/WMO, 2018). The distance from the catchment to these stations is 100–150 km. For the period before 1970 we used GNIP day from Vienna and Ottawa, roughly following Meinardi (1994). This yields an average ^{3}H concentration of 7.0 TU for the mixture over the last 100 years, assuming exponential decay until the measurement year 2014. For the ^{4}He subsurface production, we assumed an average accumulation rate applying for the whole study area to be 4.75×10^{-11} ccSTP/g_{H2O} per year for well fields screened below the regional Waalre aquitard in the Roer Valley Graben and 1.5×10^{-11} ccSTP/g_{H20} for well fields screened above this aquitard and in the areas outside of the Graben. These values are in the range of values derived by Blaser, Coetsiers, et al. (2010) for a nearby aquifer system, and we tested this assumption using the ^{14}C apparent ages and measured $^{4}He_{rad}$ concentrations of our study (see Supporting Information, Section S3). Using these accumulation rates, an average $^{4}He_{rad}$ concentration was calculated for each of the 5 DTTDM age classes (Table 1). For the evaluation of the ^{14}C apparent ages of the well field samples, we assumed linear mixing of the "average age" of all water within the DTTDM age class which yields a 17,500 years age for the DTTDM age class 10,000–25,000 years (Table 1). The average annual air temperature for the period 15–50 ka years was based on Isarin et al. (1998), Vandenberghe et al. (1998), Vandenberghe et al. (2004) and Renssen et al. (2007) and on NGT records from Stute and Deak (1989), Corcho Alvarado et al. (2009), Blaser, Kipfer, et al. (2010) and Varsanyi et al. (2011) that indicated a 9–10 °C temperature increase between the Last Glacial Maximum (LGM) and present and a 4–5°C temperature difference between pre-LGM and present. The average for the 0–14 ka temperature was based on Affolter et al. (2019) which was scaled towards the Dutch annual average temperatures. For the present situation an annual average recharge temperature of 10 °C was estimated using the soil temperature data in Jacobs et al. (2011). Section S4 and Figure S7 and in the Supplementary Information summarize and illustrate the estimated past recharge temperatures and the averages that were used for the DTTDM age classes.

In choosing a shape-free age distribution model, we opted to limit the amount of bins (5) to the limited amount of tracers (4) in order to overcome problems of over-parameterization (Leray et al., 2016; Massoudieh et al., 2014; McCallum et al., 2017; Visser et al., 2013). The DTTDM therefore consists of a discrete number of 5 bins that were filled with 5% increments of one of the 5 age classes, together representing 10,626 unique mixes that represent the possible travel time distributions (Visser et al., 2013). The distributions (100%,0%,0%,0%,0%) and (0%,0%,0%,0%,100%) form the youngest and oldest possible age distribution respectively. Subsequently, the concentration of the tracer in the mixture is calculated by linear mixing of the concentrations of the 5 DTTDM age classes, weighing for the proportion of the age classes in each of the bins. For example: one of the 10,626 distributions might have 5% water younger than 100 years (1st bin), 10% between 100–1,000 years (2nd bin), 60% between 1,000–10,000 years (3rd bin), 25% 10,000–25,000 years (4th bin) and 0% > 25,000 years (5th bin). For this hypothetical distribution we find the following tracer concentrations: 0.35 TU tritium, NGT 7.7 °C, 3.64×10^{-7} ccSTP g^{-1} ^{4}He and an average age of 7,730 years. All the tracer concentrations of the possible 10,626 distributions were then compared with the measured ^{3}H and ^{4}He concentrations of the sample and the NGT and ^{14}C apparent age that were derived for the sample. Subsequently, the best-fit models were identified based on the deviations between modeled and measured concentration using a chi-square approach, that weighs the measurement uncertainty of the measured tracer concentration:

$$\chi^2\,{}^3\mathrm{H} = \left({}^3\mathrm{H}_{\mathrm{DTTDM}} - {}^3\mathrm{H}_{\mathrm{sample}}\right)^2 / \left({}^3\mathrm{H}_{\mathrm{uncertainty}}\right)^2$$

$$\chi^2\,{}^4\mathrm{He} = \left({}^4\mathrm{He}_{\mathrm{DTTDM}} - {}^4\mathrm{He}_{\mathrm{sample}}\right)^2 / \left({}^4\mathrm{He}_{\mathrm{uncertainty}}\right)^2$$

$$\chi^2\,\mathrm{NGT} = \left(\mathrm{NGT}_{\mathrm{DTTDM}} - \mathrm{NGT}_{\mathrm{sample}}\right)^2 / \left(\mathrm{NGT}_{\mathrm{uncertainty}}\right)^2$$

$$\chi^2\mathrm{apparent\ age} = \left(\mathrm{average\ age}_{\mathrm{DTTDM}} - {}^{14}\mathrm{C\ apparent\ age}_{\mathrm{sample}}\right)^2 / \left({}^{14}\mathrm{C\ apparent\ age}_{\mathrm{uncertainty}}\right)^2$$

$$\chi^2{}_{\mathrm{sample}} = \chi^2\,{}^3\mathrm{H} + \chi^2\,{}^4\mathrm{He} + \chi^2\mathrm{NGT} + \chi^2\,\mathrm{apparent\ age}$$

We choose the average of the 50 best-fit models to determine the average age distribution that fits the data best and used these 50 models to calculate a standard deviation for the proportions of the 5 age classes for each of the individual well fields.

We tested the robustness of the DTTDM approach using a simple sensitivity analysis where we compared the results of the base case model runs with a number of alternative setups. The aim of the sensitivity analysis was to test whether the DTTDM approach is robust and whether uncertainties are sufficiently small to assess and order the well fields on the basis of their age distributions. Alternative model run 1 assessed the uncertainties involved in the estimated temperature series assuming a slightly warmer early Holocene in line with Marcott et al. (2013, see Section S4 in the Supplementary Information). The resulting alternative DTDDM input has slightly warmer temperatures for the age classes 25,000–50,000 years (5.5 vs. 5 °C), 10,000–25,000 years (2.7 vs. 2.2 °C), 1,000–10,000 years (10.3 vs. 9.6 °C) and late Holocene (9.8 vs. 9.3 °C). Alternative model runs 2 and 3 tested the effects of a 1.5 times higher and lower He production rate. In model run 4 we analyzed an alternative ^{3}H concentration for the first age class based on GNIP data from Koblenz instead of Emmerich and Groningen, and in alternative model run 5 we tested a two times milder constraint for the uncertainty around the estimated apparent ages. Finally, we examined the effects of subsequently dropping the NGT, ^{4}He, ^{14}C apparent age tracers in the model runs 6, 7 and 8.

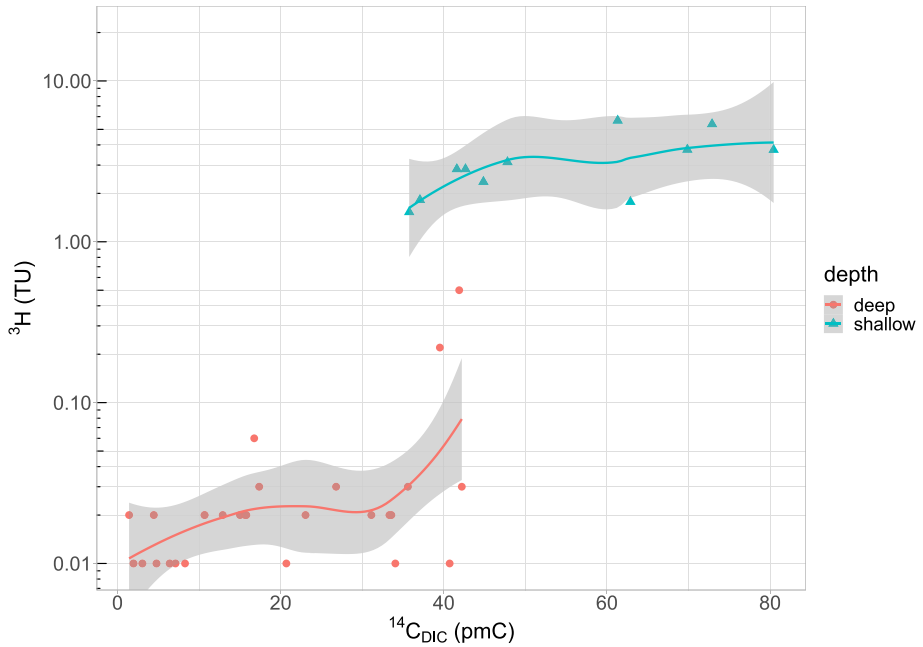

Figure 2. Tritium (TU) versus $^{14}C_{DIC}$ (% modern carbon, pmC). Labels denote the average depth of the well field. Deep: ≥ 50 m below surface. Shallow: <50 m below surface.

3. Results and Discussion

3.1. Patterns of Major Chemistry, Isotopes and Noble Gases

3.1.1. Radioactive Isotopes

The 39 well fields cover a wide range of tritium concentrations and $^{14}C_{DIC}$ activities (Figure 2, Table S1). Clearly, 3 sets of well fields can be distinguished: (a) well fields with ^{3}H concentration > 0.1 TU and ^{14}C activities above 35% pmC, (b) well fields with ^{3}H concentrations ≤ 0.03 TU and $^{14}C_{DIC}$ activities below 30%, and (c) well fields that fall between these two end members with $^{14}C_{DIC}$ between 30 and 45 pmC and ^{3}H <0.1. The detection of low, but measurable, concentrations of ^{3}H in waters that are clearly depleted in $^{14}C_{DIC}$ is no surprise. After all, the samples represent mixtures at the pumped well fields, which may abstract a small amount of young water that has infiltrated in the direct vicinity of the pumping wells. The precise determination of ^{3}H allows estimation of this contribution of modern water in Section 3.3. Typically, the first group of samples represents water that has a significant contribution of post-1950 water in the mixture. This is related to the shallower depth of pumping; all these well fields have an average depth of less than 50 m with one exception which is just below this depth. The second group has a negligible contribution of young water and large parts of the mixtures have undergone radioactive decay of ^{14}C or uptake of dead carbon. Most of these well fields have an average depth over 100 m or 150 m, which means that they are screened below a regional aquitard (see Section 3.3). Samples from the intermediate, third group are also typically from well fields screened between 50 and 150 m depth yet seem to have a small contribution of young post-1950 water. All these well fields are situated in the western part of our study area, outside the graben structure, where the regional aquitard that exists in the graben is less developed.

3.1.2. Major Chemistry

All but three of the water works in Brabant pump water with a Ca-Mg-HCO_3 signature, and are characterized by a (Mg + Ca)/HCO_3 ratio of 0.93: 1 in meq/l (see Supporting Information, Figure S2). The ratio indicates that the dissolution of Ca-Mg-carbonates by carbonic acid is the major process determining the carbon chemistry. Exceptions to this general rule are the well fields BW4, BW29, and BW39. These three well fields are high in ^{3}H (3.73–5.39 TU) and have a $CaSO_4$ signature and an alkalinity <1 meq/l, pointing towards recent human influence and the absence of carbonates in the catchment areas of these wells. Given the mere absence of carbonates in the shallower deposits in the Noord-Brabant region and the general increase

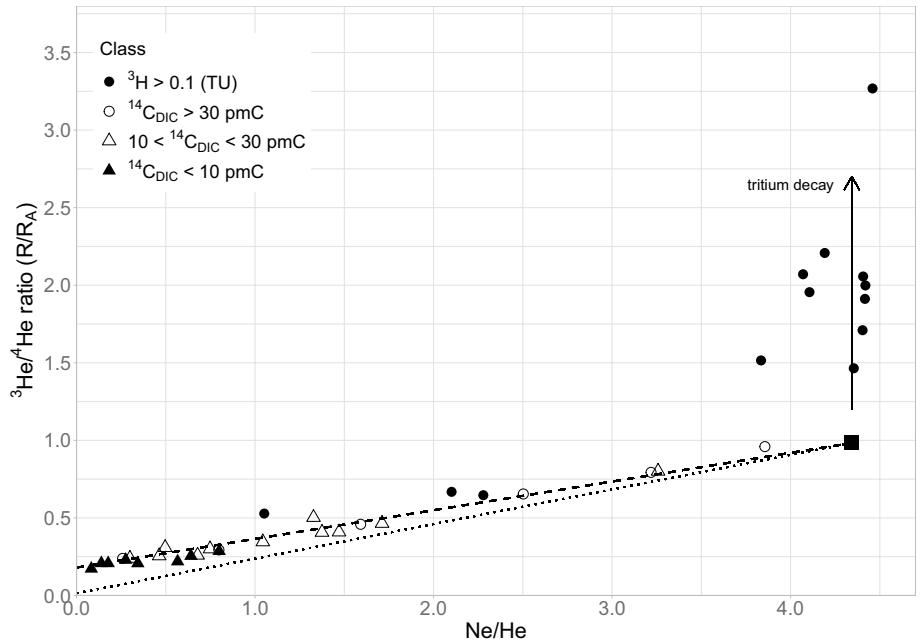

Figure 3. ^{3}He/^{4}He ratio (R) normalized to the atmospheric ratio (R_A) plotted against the ratio of Ne over He for the 39 well fields. Symbols denote classes based on ^{3}H and $^{14}C_{DIC}$. The black square indicates atmospheric equilibrium ratios of the ratios of Ne/He (= 4.34 for 10°C) and ^{3}He/^{4}He (R/R_A = 0.983). The dotted line represents binary mixing between recently infiltrated groundwater and a sample that is closed off from the atmosphere and where concentrations solely are determined by radiogenic processes producing ^{3}He and ^{4}He. The tritium-dead well field samples plot along a line with R/R_A ~0.18 on average (dashed line).

of Ca and HCO_3 with depth (Broers, 2002; Kasse, 1988; Griffioen et al., 2013; Stuurman et al., 1989, 1996) we may safely assume that carbonate dissolution at the majority of the well fields occurred at larger depths under closed system conditions using CO_2 from the root zone as the primary source of carbonic acid in the infiltrating water. Several samples with a substantial amount of methane (CH_4 > 1.5 mg/l) typically expose the highest alkalinity and highest sum of Ca, Mg, and Na-excess (see Supporting Information, Figure S2). This points to biogenic methanogenesis as an additional source of carbonic acid. It suggests that further dissolution of carbonates has occurred in the subsurface of the well fields that are represented by these samples (Griffioen et al., 2013; Yu et al., 2018).

3.1.3. Noble Gas Characterization

The Noble Gas Temperatures were all fitted applying the CE excess air model (Supporting Information Table S2). Thirty-five of the 39 samples contained excess air, indicated by ΔNe values ranging between 4% and 35% (Table S2). For sample BW19, we used the ΔNe of Bremen as the Heidelberg Ne concentrations may indicate an air leak. Three samples had slight indications for a small amount of degassing (ΔNe −2 to −6%, BW4, BW5 and BW17) and one sample (BW7) had ΔNe not significantly different from zero. We assume that the degassing has happened in the aquifers itself, as previously assessed by Visser et al. (2009c) for shallow samples in the same region.

Radiogenic ^{4}He-concentrations were consistent between the two labs (R^2 = 0.995). For the samples BW20 and BW27 that were lost during noble gas analysis at Heidelberg, estimated $^4He_{rad}$ from the Bremen results were used, correcting for atmospheric and excess air derived helium based on the unfractionated air assumption (Table S2, Bremen results). The Bremen Ne, ^{3}He and ^{4}He concentrations show how the ^{3}He/^{4}He ratio (as R/R_A) and Ne/He ratio vary between the well fields (Figure 3). Here, R is the ^{3}He over ^{4}He ratio in the sample, and R_A the ^{3}He/^{4}He ratio in the current atmosphere. The dotted line between the atmospheric end member (black square) and the point on the *Y*-axis at R/R_A = 0.0145 represents binary mixing between recently infiltrated groundwater and a sample that is closed from atmosphere and where concentrations solely are determined by radiogenic processes, producing mainly ^{4}He and little ^{3}He. Typically, in the earth

crust the $^3He/^4He$ ratio is around 0.02 R_A (Aeschbach-Hertig, 2005; Hilton, 2007). Most samples that contain ^3H over 0.1 TU plot vertically above the Ne/He ratio for atmospheric equilibrium, indicating ^3He produced by ^3H decay. Contrary, samples with $^{14}C_{DIC}$ less than 30 pmC and very low ^3H plot along a mixing line between R/R_A ~0.18 and the atmospheric equilibrium. This points to the underground flux of ^4He with an approximately 10 times larger $^3He/^4He$ ratio than is expected from He production in the crust, pointing to the presence of a reservoir that is enriched in ^3He, such as the earth mantle (typically between 5 and 8 R_A), or alternatively a contribution of ^3He from neutron reactions with lithium. A lithium contribution seems to be unrealistic given the thick series of unconsolidated deposits in the rift valley as these deposits typically have little lithium to produce the required ^3He (Ballentine & Burnard, 2002). A mantle contribution seems more realistic in the tectonic setting of the RVG. The correlation between crustal production of ^4He and mantle derived fluxes of ^3He is often associated with fault systems in basin settings, and tectonic forcing and episodic seismic activity are supposed to be the dominant mechanisms for fluid transport and transfer of volatiles through fault zones in the uppermost crust (Hilton, 2007; Kulongoski et al., 2005). We infer that the Roer Valley Graben involves a similar setting as in Kulongoski et al. (2005) as the rift system is known for phases of crustal stretching and episodes of basin inversion, for example in the Paleocene and Eocene (Luijendijk, Van Balen, et al., 2011). Luijendijk et al. describe how periods of basin inversion may have led to larger permeability in the damage zone around the faults, promoting deeper circulation. The fault zones bordering the Roer Valley Graben have still been active in the Quaternary (Houtgast & van Balen, 2000). The R/R_A ratio varies over the studied well fields (~0.10 R_A to 0.25 R_A) with an indication for the higher values to be near the main fault zones. Importantly, a mantle component as indicated by the R/R_A ratios in the study area would only marginally affect the concentrations of $^4He_{rad}$ which we use as a residence time indicator in the next section; given the observed ratios ~ 98% of the ^4He is from crustal production and 2% to maximum 4% of the ^4He would result from mantle fluxes (Aeschbach-Hertig, 2005). Overall, the helium patterns suggest the presence of a somewhat enhanced crustal permeability in the rift system studied.

The Noble Gas Temperatures were used as a proxy for the average temperature of recharging meteoric water. The highest values of the NGTs (around 8.5–9.5 °C) appear in water that contains a substantial amount of ^3H, indicating a recent component of meteoric water (see Table 1 and Figures 3 and 4). Given the mixed nature of the well field samples, these values are consistent with the current mean annual air and soil temperature (~10 °C) in the province of Noord-Brabant (KNMI 2012; Jacobs et al., 2011). Sample BW5 with NGT of 11.0°C forms an exception, but its NGT is rather uncertain given the degassed nature of this particular sample.

Together, the 39 well fields reveal a clear relation between the derived NGTs and the $^4He_{rad}$ concentrations (Figure 4). High $^4He_{rad}$ concentrations ($>1.0 \times 10^{-6}$ cc/g) coincide with NGTs of 4.5 °C or lower and ^{14}C activities of less than 10% modern carbon. Samples that contain young water, as indicated by $^3H > 0.1$ TU and ^{14}C activities above 30% all plot in the range of low ^4He below 0.3×10^{-6} ccSTP/g and NGTs above 7 °C. The LOWESS smooth (Cleveland & Devlin, 1988) indicates a general curved trend of decreasing NGT with increasing ^4He concentration. Two samples (BW32 and BW38) lie out of this general trend; but these had contrasting data for He, Kr and Xe for the duplicate samples that were available. The data plotted for these wells is for the duplicate sample that corresponds to the ^4He measured in Bremen, which has significant lower Xe than the other duplicate sample. We conclude that NGTs are less reliable for these particular samples.

Moreover, the complete set of well fields reveals an inverse relation between the excess air component as indicated by ΔNe and the NGT (Figure 4). Samples that suggest cool recharge temperatures show elevated ΔNe relative to samples that exhibit NGTs close to present day recharge temperatures. NGTs of 7 °C or less coincide with samples with > 20% ΔNe. Lower recharge temperatures are typically linked to more depleted ^{18}O with all NGT < 7°C showing $\delta^{18}O_{VSMOW}$ values depleted relative to current average levels of around −7.5‰ (Figure 4). The samples with NGT > 7 °C show a range of $\delta^{18}O_{VSMOW}$ values with a substantial number of samples that are enriched relative to present-day ^{18}O in recharging water, possibly indicating evaporation processes during or after infiltration (see also Section 3.4).

3.2. Discrete Age Distributions

Using the four tracers ^4He, ^3H, NGT and ^{14}C apparent age, age distributions of the mixed waters were derived using the DTTDM model. Figure 5 summarizes the model performance for the 4 tracers. The tracers

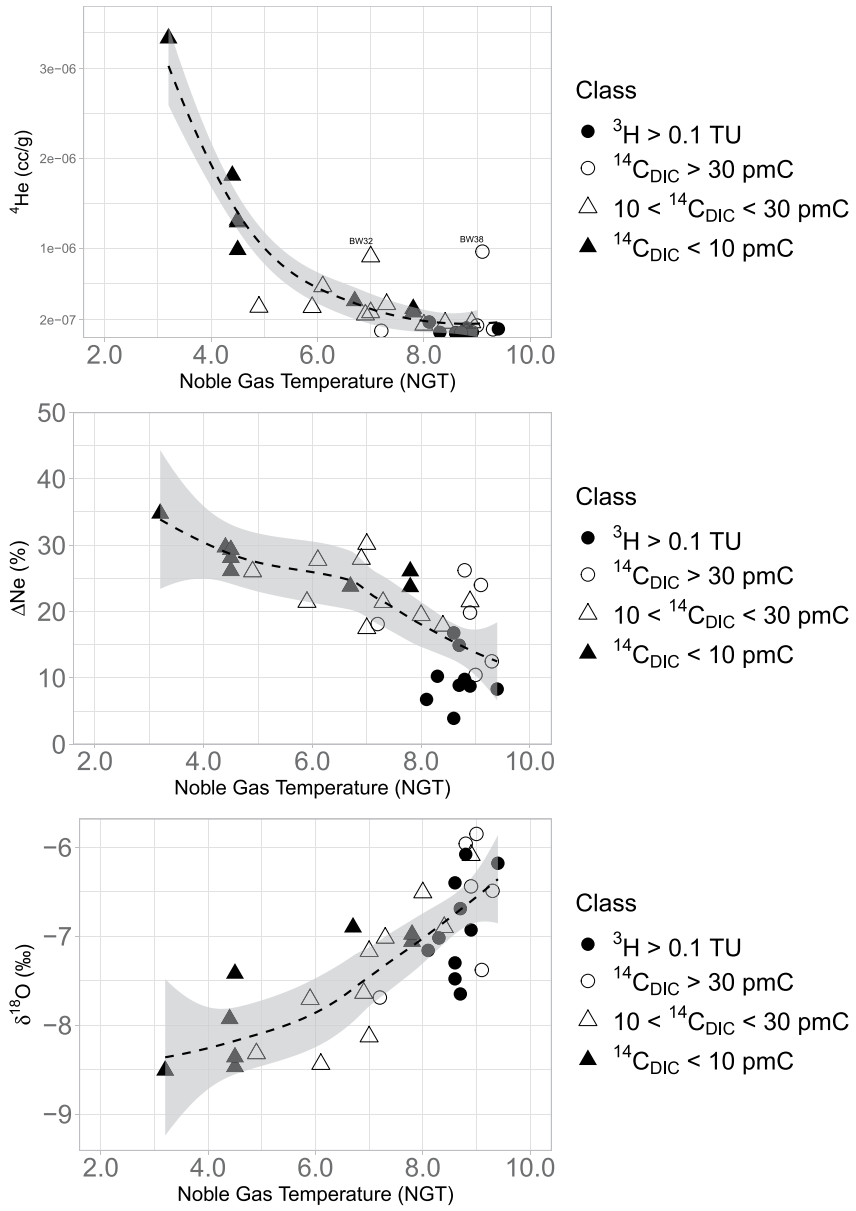

Figure 4. ^{4}He (cc g^{-1}), ΔNe (%) and δ^{18}O (‰) as a function of Noble Gas Temperatures (°C) for the 37 well fields for which the samples did not show signs of degassing. Symbols denote classes of ^{3}H and $^{14}C_{DIC}$ concentrations.

were fitted simultaneously, and the results represent a kind of optimal distribution over the 4 tracers. For samples with a recent component, the ^{3}H concentration enabled to estimate the proportion of young water; the main uncertainty is derived from the average concentration that was assumed for the first age class in the DTTDM model. Noble Gas Temperatures were also simulated satisfactorily over the whole temperature range, except for sample BW5 which was degassed and had a difficult fit for the NGT, and sample BW40 which has conflicting NGT and $^{14}C_{DIC}$ activity. The modeled ^{14}C apparent ages show good correspondence below 15,000 years but scatter at older apparent ages where the combination of $^4He_{rad}$, NGT and ^{14}C apparent ages does not always yield one unambiguous result. For some well fields, this was expected as the NGT and $^4He_{rad}$ graph of Figure 4 already showed well fields BW14, BW15 and BW18 that nicely follow the $^4He_{rad}$ - NGT trend but have low $^{14}C_{DIC}$ activity (2–7 pmC) that set them apart. For some well fields the moderate correspondence between NGT, ^{14}C apparent age and $^4He_{rad}$ led to a range of possible age distribution

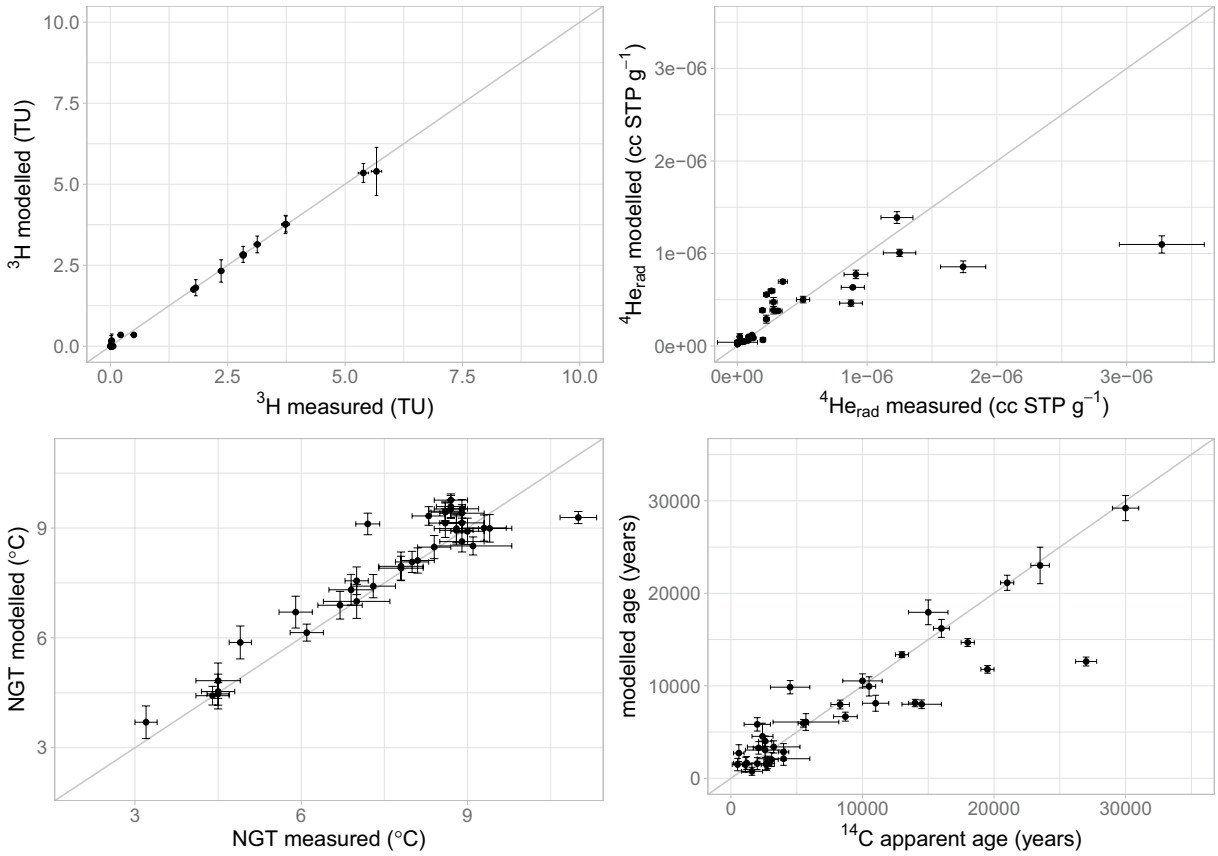

Figure 5. Performance of the DTTDM model for the 4 tracers for all 39 well fields. Gray lines represent a 1:1 ratio between measured and modeled concentrations.

models, which is visible from the standard deviations that are based on the 50 best models, indicating larger uncertainty (Supporting Information, Table S4).

Using the results of the 50 best fit models for the base case model, a resulting groundwater age distribution covering the 5 age classes was derived. Figure 6 shows the distributions of the 5 age classes over the 37 well fields of which all tracers were available. Table S4 of the Supporting Information lists the corresponding standard deviations of the proportions for each of the well fields. Subsequently, well fields were grouped based on the centroid of the age distribution into 5 "age distribution groups": Young (Y), Moderately Young (MY), Moderate age (M), Moderately Old (MO) and Old (O). The age distribution groups differ from the previously defined age classes, as they comprise different proportions of water from the 5 age classes in their distributions (Figure 6). Average tracer concentrations and standard deviations for each of the age distribution groups are summarized in Table 2. As we aimed to differentiate between the different well fields for understanding the regional age patterns and vulnerability and resilience of the well fields, we do not intend to focus on the precise proportions of the different age classes per individual well field and their uncertainty, but mainly concentrate on the ordering which is achieved using these age distribution groups and relate those to the hydrogeological situation in the study area. The age distribution groups as we defined them show a clear resemblance to the "age groups" of McCallum et al. (2017), although with different temporal scales (0–50,000 years relative to 0–1,000 years and correspondingly different tracer sets).

The sensitivity analysis reveals that varying the input curves of $^4He_{rad}$, NGT or ^3H or loosening constraints of the ^{14}C apparent ages does not fundamentally affect the ordering and grouping as presented in Figure 6 and Table S4 (see Section S6 for details). More specifically, assuming a warmer past climate only has a marginal effect on the centroids and proportions of the age distributions and very limited effects on the ordering of the well fields over the age groups Y, MY, M, MO and O (Figure S8 and Table S5). Changes in the estimated ^4He production rates have effects for the order of the centroids of the well fields of the MO age group; lower

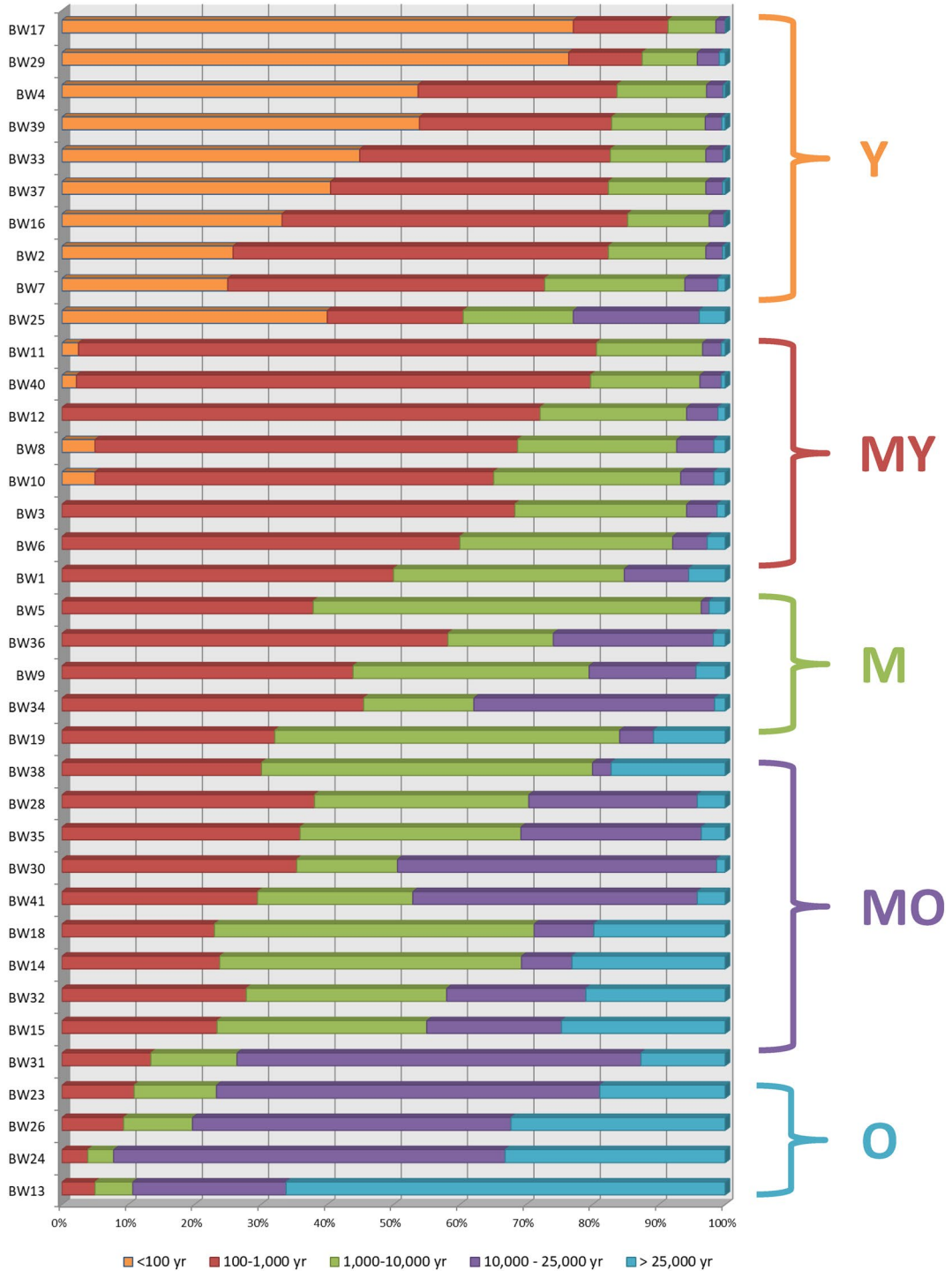

Figure 6. Discrete age distributions of the 37 well fields. Showing the distribution of water over the 5 age classes. Well fields were grouped based on the centroid of the age distribution in 5 age distribution groups (Y, MY, M, MO, and O). See Table S4 for the actual data and standard deviations of the fractions.

production rates lead to a generally older age assessment and vice versa. Altering the ^{3}H average leads to small differences in the proportions of the 6 well fields in the age group Y. Loosening constraints on the 4 tracers has effects for specific well fields; for example, loosening the ^{14}C apparent age constraints changes the order of the centroids of well fields BW5, BW14 and BW18, and affects the estimated proportions for

Table 2
Average Concentrations and Standard Deviations () Within the Distinguished Age Distribution Groups

	Age distribution group				
Tracer	Y	MY	M	MO	O
^{3}H (TU)	3.3 (1.3)	0.13 (0.15)	0.03 (0.02)	0.02 (0.01)	0.01 (0.01)
^{14}C apparent age (yrs)	2,020 (1,420)	3,340 (1,240)	7,020 (2,000)	11,400 (2,900)	22,800 (4,700)
NGT (°C)	9.3 (0.5)	8.9 (0.2)	8.4 (0.6)	6.8 (1.1)	4.4 (0.5)
^{4}He (ccSTP g^{-1})	3.3×10^{-8} (2.0×10^{-8})	5.8×10^{-8} (2.4×10^{-8})	2.1×10^{-7} (1.7×10^{-7})	5.4×10^{-7} (1.4×10^{-7})	1.1×10^{-6} (2.2×10^{-7})

BW34, BW14, BW15 and BW23. Dropping one of the 4 parameters has larger effects. For example, dropping the NGT from the models has only marginal effects on the centroids of the distributions but has a substantial effect on the estimated proportions, especially for well fields of the MO and O age groups (Table S5). Dropping either $^{4}He_{rad}$ or ^{14}C apparent age has contrasting effects; dropping ^{4}He causes a shift to older age groups while dropping ^{14}C has the reverse effect for the affected well fields; these effects are most pronounced for the well fields in the age groups MO and O.

From the sensitivity assessment, we concluded that the DTTDM approach is robust when all 4 tracers are included and we determined that the differences between the alternatives and the base model are sufficiently small to assess and order the well fields on the basis of their age distributions and use the results for a hydrogeological assessment. More specifically, for wells that were categorized as Y and MY, dropping one of the 3 tracers NGT, $^{4}He_{rad}$ or ^{14}C apparent age would not affect the estimated proportions of the age groups, but including the ^{3}H tracer is essential. For assessing the proportions of the M, MO and O groups, NGT, $^{4}He_{rad}$ or ^{14}C apparent age are all necessary, but the exact past recharge temperatures series is not very sensitive once the NGT tracer is included. The sensitivity analysis confirms the relatively uncertain proportions and grouping of the well fields BW14, BW15 and BW18, which was also reflected in the large standard deviations of the proportions listed for the base case model (Table S4).

3.3. Interpretation of the Age Distributions in a Hydrogeological Setting

The discrete age groups that have been delimited in Section 3.2 clearly exhibit a relation with the main hydrogeological structures of the area. The hydraulic gradient in the main aquifers of both the Roer Valley Graben and the adjacent area of western Brabant is directed towards the northwest. Generally, the age groups that were distinguished conform to this gradient with water aging in the direction of groundwater flow (Figure 7). Well fields that were screened in the upper aquifers (<50 m depth) all are grouped in the Y age distribution group. These well fields have a significant contribution of water age classes <100 years and 100–1,000 years) and measurable concentrations of ^{3}H (Figure 6, Table 2, Table S4). These well fields typically pump from unconfined aquifers which are not overlain by a continuous superficial aquitard but are covered by discontinuous cover layers of eolian and local fluvial origin that do not prevent young water from recharging quickly.

3.3.1. Roer Valley Graben Groundwater Circulation

Past groundwater recharge of the Roer Valley Graben groundwater system is expected to have concentrated in the southeasterly extension of the Graben in the border region with Germany, and possibly in the southeastern part of the study area and the Dutch and Belgian parts of the Campine Plateau (Blue arrows in Figure 7). The MO group groundwater age distributions in the center of the Graben point to a large contribution of water that recharged during the Pleistocene era and before and after the Last Glacial Maximum. The MO group waters are drawn from the lower Waalre and Kieseloolite aquifers between depths of 100 and 300 m, which are separated from the upper Sterksel aquifer by the regional Waalre-1 and Kieseloolite-1 aquitards (diagonally striped in Figure 7). Apparently, the confining Waalre-1 aquitard has prevented recharge of younger water which is confirmed by regional groundwater flow models describing the current flow circulation and age structure (Grift et al., 2012). The oldest water in the Graben is situated in the very northwest and along the northeastern flank of the Peel Boundary Fault zone. These group O waters were characterized by lower NGT and elevated $^{4}He_{rad}$ relative to water from the MO group (Table 2). Interestingly,

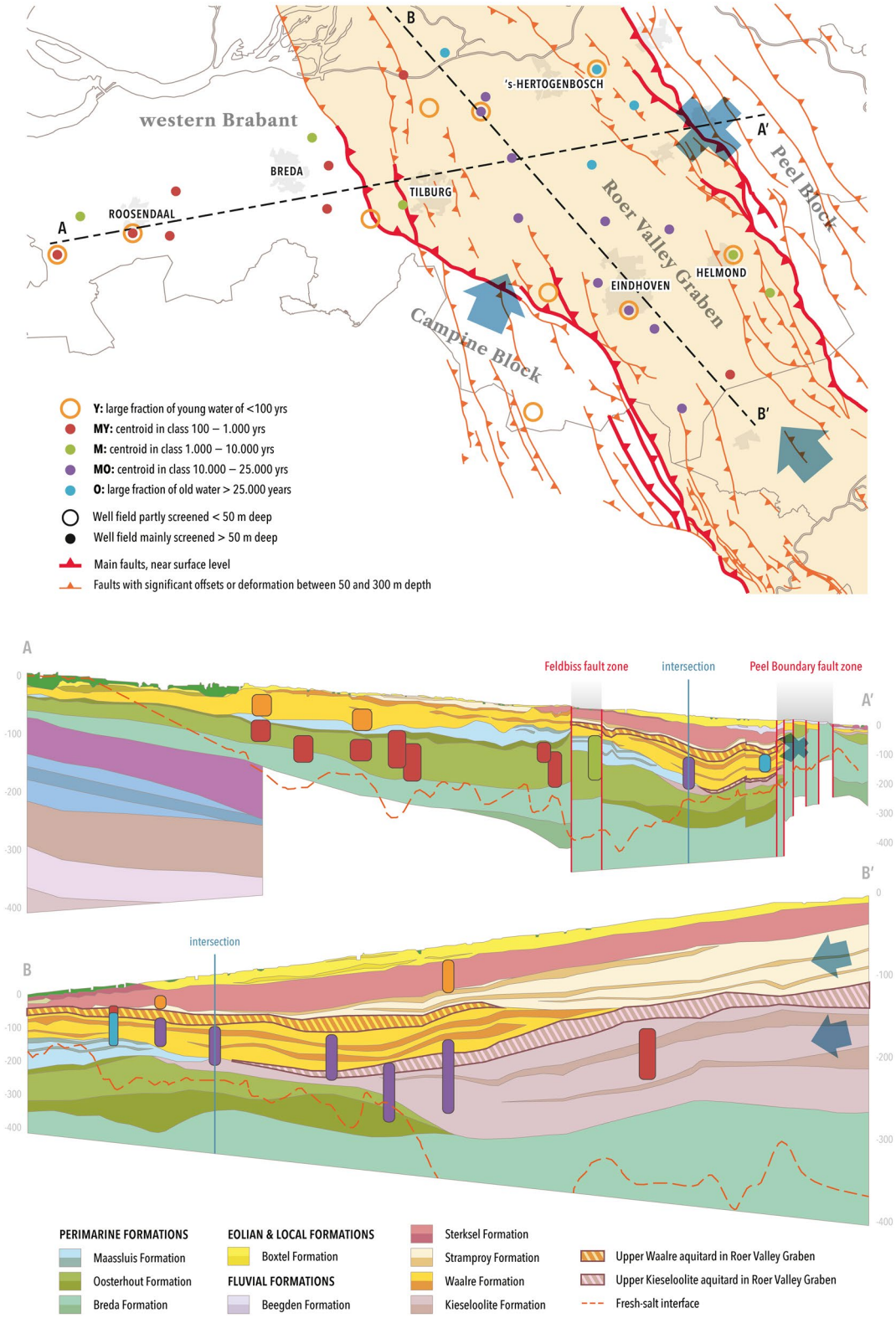

Figure 7. Spatial distribution of the age distribution classes showing the well fields in their hydrogeological setting. Roer Valley Graben indicated in yellow shade on the map. Arrows denote the main directions of groundwater flow. The blue cross indicates blocked flow by the sealed Peel Boundary Fault which prevents water from the higher altitude Peel Block to flow into the Roer Valley Graben. MY waters mainly occur in the Oosterhout Formation in western Brabant. Age classes MO and O only occur in the Roer Valley Graben below the Waalre-1 and Kieseloolite-1 aquitards (diagonal stripes), showing a age gradient from SE to NW. Darker colors in the legend indicate aquitards within the Formation, lighter colors indicate aquifers.

the pumping depth of these well fields is similar or shallower (100–200 m) than the well fields in the center of the Graben, which suggest that flow velocities are small and recharge to this northwesterly region is limited. The northeast part of the Roer Valley Graben is the region where the strongest tectonic sinking occurred which resulted in the thickest sequence of Quaternary sediments and where the Waalre-1 aquitard is most developed; the area around well fields BW23 and BW24 is considered to be a marginal through which is delineated by the Peel Boundary fault and an antithetic fault to the west of it (Luijendijk, Van Balen, et al., 2011). We interpret the occurrence of well fields with a large proportion of water >25,000 years in this northeastern part of the Graben to be the combined result of the sealed properties of the Peel Boundary Fault zone (blue cross in Figure 7) that borders the Graben structure on the eastern side and the thick development of the Waalre-1 confining layer in the Graben itself. The Peel Boundary fault zone is known to have been active in the late Pleistocene and Holocene, leading to moderate earthquakes in the recent past (Van Wees et al., 2014; Buijze et al., 2019). The fault gives rise to the phenomenon of "wijst," which is the upward seepage of water on the eastern side of the fault due to the decreased hydraulic conductivity of the sealed fault which acts as a barrier towards horizontal groundwater flow (Bense, 2002; Bense, Van den Berg & Van Balen, 2013; Bense et al., 2003). The presence of "wijst" confirms the sealed nature and the horizontal resistance to shallow groundwater flow (Lapperre et al., 2019). As the area east of the fault zone (cross at the map and in cross-section of Figure 7) has higher elevation than the Graben itself, groundwater flow would be expected to rejuvenate the water in the adjacent Graben area. Finding water with a large proportion of water of >25,000 years old at moderate depths (100–150 m) at close distance to the eastern topographical height can only be explained by high resistance to groundwater flow from the east towards the Graben. Therefore, we suggest that the Peel Boundary Fault is not only a barrier to shallow groundwater flow as indicated by the "wijst" phenomena, but also acts as a strong barrier to groundwater flow in the deeper parts of the subsurface.

3.3.2. Western Brabant Groundwater Circulation

In the western Brabant groundwater system, the groundwater flow direction is towards the northwest and the water ages in that direction. Confining layers are less developed in this region and water is primarily pumped from the Pliocene Oosterhout Formation. Here, the upper aquitard in the marine Oosterhout Formation separates the Y group waters above from the MY waters below (Figure 7). Two of these well fields, BW8 and BW 10, have a small contribution of ~5% young water that has apparently leaked from the upper aquifer through the leaky aquitard at the top of the Oosterhout Formation, the so-called Wouw member, which is situated above the pump screens (TNO-GSN, 2021).

In summary, the age distribution groups that were identified based on the multi-tracer approach improved the understanding of the regional groundwater circulation in the region and confirms the large effects of fault structures and aquitards, complementing existing information of surface phenomena such as "wijst." This shows that the DTTDM age grouping approach is suitable in a rather complex setting as the Roer Valley Graben. The Graben setting is complex in the sense that it represents a typical lowland valley system without large natural head gradients and with unidentified interactions between deeper and shallower aquifers due to pumping and intense superficial drainage of the upper aquifers. A such, the setting is contrary to well-studied systems of dipping aquifers with fully delineated source zones and a strongly confining cap rock preventing vertical interactions and disturbance of the longitudinal aging of water along the flow paths (e.g., Blaser, Kipfer, et al., 2010; Pétré et al., 2016). Especially the information about the He isotopes and the NGT helped to identify the age groups and to identify the large proportion of Pleistocene aged waters in the study area.

3.4. Paleoclimate Signals

By introducing the NGT as one of the tracers in the assessment of the age distributions, paleoclimate was implicitly considered in our study. For our well fields, NGT appeared to be strongly inversely related to ΔNe as indicator of excess air, and positively related to the $\delta^{18}O_{VSMOW}$ (Figure 4). The latter is expected as colder precipitation generally leads to depleted ^{18}O in recharging water (e.g., Jasechko, 2016, 2019), but the inverse relation with ΔNe came as a surprise. The elevated ΔNe suggests that the excess air fraction in waters with low recharge temperatures is elevated, which may be related to a larger water level amplitude (Aeschbach-Hertig & Solomon, 2013; Aeschbach-Hertig et al., 2002; Ingram et al., 2007; Klump et al., 2008).

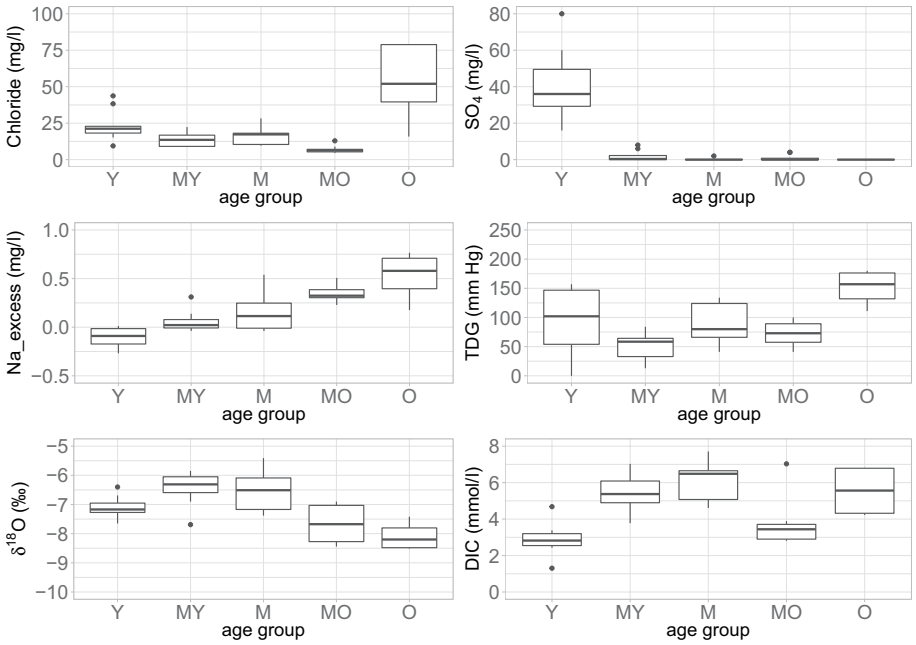

Figure 8. Boxplot of (a) chloride, (b) sulfate, (c) excess-Na, (d) Total Dissolved Gas Pressure, (e) $\delta^{18}O$ and (f) DIC concentrations for the 5 distinguished age distribution groups.

This suggests a more extreme climate with larger differences between dry and wet periods, as was previously reported by Corcho Alvarado et al. (2009). We postulate that larger water level amplitudes may also be related to the distance to the drainage basis of the groundwater systems, which we defined as the deepest water level that could be expected without artificial pumping of the groundwater and which currently conforms to average present sea level. This drainage basis shifted over hundreds of kilometers due to the significant lowering of the sea level of 120–130 m before and during the Last Glacial Maximum (Blaser, Coetsiers, et al., 2010, Table 2). As a result, the altitude differences between the points of recharge and the drainage basis increased substantially during the LGM enabling larger water table fluctuations in a more extreme climate. During the LGM, the land ice mass extended approximately to NE Germany and Eastern Denmark, at ~250 km NW of our study area, outside the reach of glacial melt water. As such, recharge by precipitation before and during the LGM is consistent with the range of ΔNe values reported in our samples (Klump et al., 2008). The hydrological changes that influenced the ΔNe are confirmed by the distinctly different low chloride concentrations (4–6 mg/l) that were measured in the age group MO (Figure 8a). This coincides with the periods just before and after the LGM. We attribute these low concentrations to the large distance of the study areas to the North Sea, of which the coastline shifted some 600 km northwest due to the sea level decline during the LGM (Blaser, Coetsiers, et al., 2010; Hijma et al., 2012; Vos, 2015). We suggest that sea spray did not reach the recharge areas of the water from that epoch and there was no vegetation that would evaporate and concentrate chloride during recharge. This seems to be confirmed by the relatively low DIC concentrations in water of the MO group, indicating a sparser vegetation and lower levels of soil CO_2 leaching to groundwater. Under this hypothesis, the relatively low DIC concentrations of "LGM waters" in a mixture might add to extra uncertainty of the ^{14}C apparent ages of well samples that mix over the LGM era, as the low-DIC LGM component would yield an underrepresentation of the LGM-^{14}C part of the mixture. This may lead to an underestimation of the ^{14}C apparent age when LGM water is mixed with post-LGM water before the water is pumped at the well field, or an overestimation of the ^{14}C apparent age after mixing with pre-LGM waters.

The age group O shows elevated chloride, Na-excess and Total Dissolved Gas Pressures which we attribute to the long time scales that seems to have favored diffusive transport of sodium and chloride from low permeability layers into the aquifers and subsequent exchange of Ca from the recharging water with Na on the exchange complex of the aquitards, or alternatively the weathering of Na-silicates during the aging of the water. Given the low concentrations of <3.5 mg/l CH_4 in those waters, we hypothesize that the elevated gas

pressure must be related to elevated N_2 in the water as this cannot be explained by the CO_2 and CH_4 partial pressures (Table S1, e.g., Ballentine & Lollar, 2002)). This may also be illustrative for the enrichment of gases from the deeper subsurface over time, for which the high $^4He_{rad}$ concentrations are another proxy

Contrary to the depleted $\delta^{18}O_{VSMOW}$ values of age group O, $\delta^{18}O_{VSMOW}$ values of age groups MY and M are typically elevated to present-day values in precipitation and seem indicative of the recharge under raised peat bogs during the late Holocene, an hypothesis which is supported by the elevated methane and $^{13}C_{DIC}$ for which we correct in the calculation of the ^{14}C apparent age (see Supporting Information, Section S2). Two main processes may explain these elevated $\delta^{18}O$ values: open water evaporation of surface water stored in fens and pools within the peat bog areas and/or mixing of diverging $\delta^{18}O$ values between summer and winter precipitation before actual recharge to groundwater (see also Glasbergen & Mook, 1982). Well fields of the MY and M groups are indeed concentrated in areas with known Holocene peat bog existence, such as the western and southeastern parts of Noord-Brabant (Leenders 1989, 1996; Vos, 2015). The waters from the Holocene epoch show chloride concentrations between 10 and 20 mg/l, which are in accordance with present day chloride concentrations under natural vegetation and resemble the effect of salt spray from the nearby North Sea (Stuyfzand, 1993). In contrast, the well fields of group Y exhibit anthropogenically elevated chloride and sulfate concentrations due to inputs from diffuse agricultural, industrial and urban sources during the last 100 years (Visser, Broers et al., 2009; Zhang et al., 2009).

3.5. Merits of Complementary Tracers

The current study builds on recent advances in the assessment of groundwater age distributions using multi-tracer data sets and shape-free age distribution models (Massoudieh et al., 2014; McCallum et al., 2017; Visser et al., 2013) but at longer temporal scales including groundwater recharge and circulation that started during the late Pleistocene. The age grouping that was established helped to understand the complex flow patterns in a lowland rift valley system with a relatively small hydraulic head gradient. The tracer set that was used to unravel the age distributions has some limitations, that were determined by available budgets and lab capacity. Clearly, further constraints of the proportion of water aged between 100 and 1,000 years in the Y, MY and M groups would benefit from the analysis of ^{39}Ar as an additional tracer (Corcho Avarado et al., 2007; Loosli, 1983; McCallum et al., 2017; Oeschger et al., 1974; Sültenfuß et al., 2011; Visser et al., 2013). For example, an analysis of ^{39}Ar or the sampling of multi-level observation wells over the complete depth range, as was previously done in Holten (Visser et al., 2013) would be required to confirm or reject our hypothesis that the water pumped in the MY age group integrates over the whole depth range of the available aquifers in this region. Currently, the lab capacity for analyzing a large set of samples for ^{39}Ar is limited worldwide, but this may change during the coming decade. However, the set of tracers that we applied in the current study is ready for practical application in larger regional studies and especially the NGT appeared to be a crucial tracer for the time scales involved in the groundwater circulation in our study area. For our study, we did not consider using chlorofluorocarbons (CFCs, Busenberg & Plummer, 1992; Hinsby et al., 2007; Laier, 2014; Sebol et al., 2007) for characterizing the modern waters of age group Y, because the earlier work of Visser, Schaap, et al. (2009) showed signs of degradation for CFC-11, CFC-12 and even CFC-13 in the Dutch settings which are dominated by anoxic and often methanogenic groundwater below 10–20 m depth (Griffioen et al., 2013; Visser, Schaap, et al., 2009; Yu et al., 2018; Zhang et al. 2009, 2012). The use of sulfur-hexafluoride (SF_6, Busenberg & Plummer, 2000) may however add further value as degassing did not typically affect the samples in the current study. Moreover, adding a tracer for the oldest parts of the age distributions would help to unravel the ambiguity that is observed between the modeling of the $^4He_{rad}$ concentrations using a regionally fixed production rate and the modeling of ^{14}C apparent ages. We suggest that the measured $^{14}C_{DIC}$ activities may underestimate the age of especially the water in the O age group, but additional tracers such as ^{81}Kr and ^{36}Cl would be needed to confirm this hypothesis. The consistent ratios of $^3He/^4He$ reported by the R/R_A ratio of Figure 3 suggest that the processes determining the $^4He_{rad}$ accumulation are valid for the whole study region, because mantle He would only add 2%–4% of the extra He from radiogenic sources, assuming a ratio R/R_A of 6–8 for mantle He (Hilton, 2007). To confirm this hypothesis, further proof is needed, for example, by measuring ^4He concentrations and $^3He/^4He$ ratios in individual pumping wells in transects perpendicular to the main faults.

3.6. Implications for Sustainable Groundwater Management

The heavily used Roer Valley Graben aquifer system forms one of the groundwater resources under the combined stress from anthropogenic contamination of shallower aquifers, primarily by intensive livestock farming (Visser et al., 2007; Zhang et al., 2009), and an ongoing shift towards the mining of a paleo groundwater resource due to increasing water demands (e.g., Schilling et al., 2015; Bierkens & Wada, 2019; de Jong et al., 2020). The shift is apparent as many of previously active shallower well fields have been closed during the last 30 years, especially because of increasing sulfate and trace metal concentrations (e.g., Zhang et al., 2009), a process that is also visible in the well fields of the age group Y (Figure 8). With the age distributions of all the extracted water for public drinking water supply qualitatively constrained, we now estimate the current combined age distribution of all the 0.18 km^3 water that is annually abstracted for drinking water production in this part of the Netherlands; 9% is recently infiltrated modern water, 56% is of Holocene age and 35% of Pleistocene age. We consider it wise to evaluate how long the deeper paleowater resource would sustain its use for drinking water production for humans and cattle, irrigation of farmlands, storage of heat and the extraction of geothermal energy, given the volumes available, the storage coefficients and the recharge rates involved. For that reason, we recommend using the identified age groups as targets for groundwater flow modeling and water balance studies. For example, the presence of O group water in the northeastern marginal through of the Roer Valley Graben near well fields BW23 and BW24 puts constraints at modeled hydraulic conductivities of the Peel Boundary Fault zone fault zone to the east, implying that the region could be relatively vulnerable for overexploitation and salinization. In using the age information as a target for groundwater flow models, it should be realized that the age distributions that are manifest today are partly the result of a slow groundwater circulation from the past, while there are signs that the increase and deepening of abstractions for irrigation and drinking water have reversed vertical head gradients and groundwater flow directions and perhaps recharge areas (Buma et al., 2021; Delsman et al., 2014). First signals of small proportions of modern water were determined in the mixture of the waters of the MY group well fields, which might indeed indicate that the age distribution of some of these well fields may not yet be at steady state. Therewith, the proportion of modern water may increase with time as the younger water penetrates deeper into the aquifers under the current pumping regimes.

4. Conclusions

Assessing age distributions of large-scale drinking water production wells is beneficial for understanding the evolution of water quality in time and characterizing the vulnerability of well fields and may support water producers to ensure customer trust in the source of the drinking water. Our data set suggests that evaluation of noble gases together with chemical and isotope tracers is effective in unraveling spatial and temporal patterns of water quality at the scale of large well fields used for drinking water supply, and that the application of an age histogram approach such as DTTDM helps to identify well fields with common age characteristics and paleoclimate influence. Applying the 4 tracers ^3H, $^4He_{rad}$, $^{14}C_{DIC}$ and NGT in the DTTDM modeling led to a sufficiently robust ordering and grouping of the age distributions of the well fields; the so-called "age distribution groups." The grouping of the well fields appeared to be rather insensitive to changes in the input series of the ^4He production, records of tritium in precipitation and the reconstruction of past Holocene and Pleistocene recharge temperatures, thus enabling their use in the hydrogeological assessment of the regional circulation. We did not intend to focus on the precise proportions of the different age classes per individual well field and their uncertainty, but mainly concentrated on these age groups and related them to the hydrogeological situation in the study area. The results indicated that the pumping-induced mixing may involve a wide range of water ages, even though the production wells are often partially penetrating; we relate this to the large abstraction volumes of the centralized well fields which tend to integrate water over a considerable depth range. The analysis of these large production well fields also suggests that measured $^{14}C_{DIC}$ activities in pumped wells could well be the implicit result of mixing of waters ranging between 2,000 and 35,000 years old in unknown proportions, instead of being discrete ages with a limited variance as would be observed from sampling short-screened observation wells. We believe that the grouping of the age of well fields will be supportive for optimizing strategies for the sustainable use of groundwater at the supra-regional scale, allowing to evaluate the vulnerability of these fields in relation

to contaminants recharging at the surface and to decide whether designated protection of catchment areas would be a sensible and cost-effective approach.

Conflict of Interest

The authors declare that there is no conflict of interest.

Data Availability Statement

The meta data of the 39 well fields, the macro chemistry data and the data of the noble gases and carbon, hydrogen and oxygen isotope tracers used for assessing the paleoclimate signals and age distributions in the study are available at Zenodo via https://doi.org/10.5281/zenodo.4945430 under license CC BY-NC-ND 4.0 (Broers et al., 2021).

Acknowledgments
This study was partly funded through the GEOERA RESOURCE project, which has received funding from the European Union's Horizon 2020 research and innovation program under grant agreement No 731166. We thank Jean-Raynald de Dreuzy and two anonymous reviewers for their comments and suggestions which helped to improve an earlier version of the manuscript.

References

Aeschbach-Hertig, W. (2005). A comment on "Helium sources in passive margin aquifers-new evidence for a significant mantle 3He source in aquifers with unexpectedly low in situ $^3He/^4He$ production" by MC Castro [Earth Planet. Sci. Lett. 222 (2004) 897–913]. *Earth and Planetary Science Letters*, *240*(3), 827–829. https://doi.org/10.1016/j.epsl.2005.09.052

Aeschbach-Hertig, W., Beyerle, U., Holocher, J., Peeters, F., & Kipfer, R. (2002). Excess air in groundwater as a potential indicator of past environmental changes. In International Atomic Energy Agency (Ed.), *Study of environmental change using isotope techniques*. Proceedings of international conference held in Vienna, Vienna, 23 - 27. ISBN 92-0-116402-5

Aeschbach-Hertig, W., El-Gamal, H., Wieser, M., & Palcsu, L. (2008). Modeling excess air and degassing in groundwater by equilibrium partitioning with a gas phase. *Water Resources Research*, *44*, W08449. https://doi.org/10.1029/2007WR006454

Aeschbach-Hertig, W., & Gleeson, T. (2012). Regional strategies for the accelerating global problem of groundwater depletion. *Nature Geoscience*, *5*, 853–861. https://doi.org/10.1038/ngeo1617

Aeschbach-Hertig, W., Peeters, F., Beyerle, U., & Kipfer, R. (1999). Interpretation of dissolved atmospheric noble gases in natural waters. *Water Resources Research*, *35*(9), 2779–2792. https://doi.org/10.1029/1999wr900130

Aeschbach-Hertig, W., Peeters, F., Beyerle, U., & Kipfer, R. (2000). Paleotemperature reconstruction from noble gases in ground water taking into account equilibration with entrapped air. *Nature*, *405*(6790), 1040. https://doi.org/10.1038/35016542

Aeschbach-Hertig, W., & Solomon, D. K. (2013). Noble gas thermometry in groundwater hydrology. In *The noble gases as geochemical tracers* (pp. 81–122). Springer. https://doi.org/10.1007/978-3-642-28836-4_5

Affolter, S., Häuselmann, A., Fleitmann, D., Edwards, R. L., Cheng, H., & Leuenberger, M. (2019). Central Europe temperature constrained by speleothem fluid inclusion water isotopes over the past 14,000 years. *Science Advances*, *5*(6), eaav3809. https://doi.org/10.1126/sciadv.aav3809

Bakker, M., & Hemker, K. (2002). A Dupuit formulation for flow in layered, anisotropic aquifers. *Advances in Water Resources*, *25*(7), 747–754. https://doi.org/10.1016/s0309-1708(02)00074-x

Ballentine, C. J., & Burnard, P. (2002). Production of noble gases in the continental crust. In D. Porcelli, C. J. Ballentine, & R. Wieler (Eds.), *Noble gases in geochemistry and cosmochemistry* (Vol. 47, p. 481–538). Mineralogical Society of America. https://doi.org/10.1515/9781501509056-014

Ballentine, C. J., & Hall, C. M. (1999). Determining paleotemperature and other variables by using an error-weighted, nonlinear inversion of noble gas concentrations in water. *Geochimica et Cosmochimica Acta*, *63*(16), 2315–2336. https://doi.org/10.1016/s0016-7037(99)00131-3

Ballentine, C. J., & Lollar, B. S. (2002). Regional groundwater focusing of nitrogen and noble gases into the Hugoton-Panhandle giant gas field, USA. *Geochimica et Cosmochimica Acta*, *66*(14), 2483–2497. https://doi.org/10.1016/s0016-7037(02)00850-5

Banerjee, A., Person, M., Hofstra, A., Sweetkind, D., Cohen, D., Sabin, A., et al. (2011). Deep permeable fault–controlled helium transport and limited mantle flux in two extensional geothermal systems in the Great Basin, United States. *Geology*, *39*(3), 195–198. https://doi.org/10.1130/g31557.1

Bense, V. (2002). Hydrogeologische karakterisering van breukzones in Zuidoost-Nederland. *Stromingen*, *8*, 17–30.

Bense, V. F., Gleeson, T., Loveless, S. E., Bour, O., & Scibek, J. (2013). Fault zone hydrogeology. *Earth-Science Reviews*, *127*, 171–192. https://doi.org/10.1016/j.earscirev.2013.09.008

Bense, V. F., Van Balen, R. T., & De Vries, J. J. (2003). The impact of faults on the hydrogeological conditions in the Roer Valley Rift System: An overview. *Netherlands Journal of Geosciences*, *82*(1), 41–54. https://doi.org/10.1017/s0016774600022782

Bense, V. F., Van den Berg, E. H., & Van Balen, R. T. (2003). Deformation mechanisms and hydraulic properties of fault zones in unconsolidated sediments; the Roer Valley Rift System, The Netherlands. *Hydrogeology Journal*, *11*(3), 319–332. https://doi.org/10.1007/s10040-003-0262-8

Bethke, C. M., & Johnson, T. M. (2002). Paradox of groundwater age. *Geology*, *30*(2), 107–110. https://doi.org/10.1130/0091-7613(2002)030<0107:poga>2.0.co;2

Bierkens, M. F. P., & Wada, Y. (2019). Non-renewable groundwater use and groundwater depletion: A review. *Environmental Research Letters*, *14*, 063002. https://doi.org/10.1088/1748-9326/ab1a5f

Blaser, P. C., Coetsiers, M., Aeschbach-Hertig, W., Kipfer, R., Van Camp, M., Loosli, H. H., & Walraevens, K. (2010). A new groundwater radiocarbon correction approach accounting for palaeoclimate conditions during recharge and hydrochemical evolution: The Ledo-Paniselian Aquifer, Belgium. *Applied Geochemistry*, *25*(3), 437–455. https://doi.org/10.1016/j.apgeochem.2009.12.011

Blaser, P. C., Kipfer, R., Loosli, H. H., Walraevens, K., Van Camp, M., & Aeschbach-Hertig, W. (2010). A 40 ka record of temperature and permafrost conditions in northwestern Europe from noble gases in the Ledo-Paniselian Aquifer (Belgium). *Journal of Quaternary Science*, *25*(6), 1038–1044. https://doi.org/10.1002/jqs.1391

Böhlke, J. K. (2002). Groundwater recharge and agricultural contamination. *Hydrogeology Journal*, *10*(1), 153–179. https://doi.org/10.1007/s10040-001-0183-3

Bonte, M., Geris, J., Post, V. E., Bense, V., van Dijk, H. J. A. A., & Kooi, H. (2013). Mapping surface water–groundwater interactions and associated geological faults using temperature profiling. *Groundwater and Ecosystems of IAH Series on Hydrogeology*, 81–94.

Bonte, M., Stuyfzand, P. J., Van den Berg, G. A., & Hijnen, W. A. M. (2011). Effects of aquifer thermal energy storage on groundwater quality and the consequences for drinking water production: A case study from the Netherlands. *Water Science and Technology*, *63*(9), 1922–1931. https://doi.org/10.2166/wst.2011.189

Broers, H. P. (1989). *Hydrochemistry and isotope composition of the groundwater at well field Vlierden. TNO report DGV-TNO OS-89-06-A, 37p (in Dutch)*

Broers, H. P. (2002). Strategies for regional groundwater quality monitoring. PhD Thesis, Utrecht University. Nederlandse Geografische Studies 306. Utrecht University Repository https://dspace.library.uu.nl

Broers, H. P. (2004). The spatial distribution of groundwater age for different geohydrological situations in The Netherlands: Implications for groundwater quality monitoring at the regional scale. *Journal of Hydrology*, *299*, 84–106. https://doi.org/10.1016/j.jhydrol.2004.04.023

Broers, H. P., & de Weert, J. (2015). Dating for drinking water production: Isotopes and noble gases in the mixed water of Brabant Water (In Dutch). Deltares report 1208195-000.

Broers, H. P., Heerdink, R., Visser, A., & Marsman, A. (2012).*Aquatempo: Groundwater dating for public supply wells. TNO Geological Survey of the Netherlands, TNO report 2012-R10374. (in Dutch)*

Broers, H. P., Sültenfuß, J., Aeschbach, W., Kersting, A., Menkovich, A., de Weert, J., & Castelijns, J. (2021). Paleoclimate signals and groundwater age distributions from 39 public water works in the Netherlands; Insights from noble gases and carbon, hydrogen and oxygen isotope tracers [Data set]. Zenodo repository. https://doi.org/10.5281/zenodo.4945430

Broers, H. P., & Van der Grift, B. (2004). Regional monitoring of temporal changes in groundwater quality. *Journal of Hydrology*, *296*(1–4), 192–220. https://doi.org/10.1016/j.jhydrol.2004.03.022

Broers, H. P., & Van Geer, F. C. (2005). Monitoring strategies at phreatic wellfields: A 3D travel time approach. *Ground Water*, *43*(6), 850. https://doi.org/10.1111/j.1745-6584.2005.00043.x

Buijze, L., van Bijsterveldt, L., Cremer, H., Paap, B., Veldkamp, H., Wassing, B., et al. (2019). Review of worldwide geothermal projects: Mechanisms and occurrence of induced seismicity. TNO report | TNO 2019 R100043.

Buma, J., Reindersma, R., & Broers, H. P. (2021). Harmonisation of volumes, water balances and recharge and discharge fluxes in the H3O study area. GeoERA RESOURCE deliverable 3.4. "European Union's Horizon 2020 Research and Innovation Programme Horizon2020: GeoERA Project "Resources of groundwater, harmonized at Cross-Border and Pan-European Scale".

Busenberg, E., & Plummer, L. N. (1992). Use of chlorofluorocarbons (CCl3F and CCl2F2) as hydrologic tracers and age-dating tools: The alluvium and terrace system of Central Oklahoma. *Water Resources Research*, *28*(9), 2257–2283. https://doi.org/10.1029/92wr01263

Busenberg, E., & Plummer, L. N. (2000). Dating young groundwater with sulfur hexafluoride: Natural and anthropogenic sources of sulfur hexafluoride. *Water Resources Research*, *36*(10), 3011–3030. https://doi.org/10.1029/2000wr900151

Cleveland, W. S., & Devlin, S. J. (1988). Locally weighted regression: An approach to regression analysis by local fitting. *Journal of the American Statistical Association*, *83*(403), 596–610. https://doi.org/10.1080/01621459.1988.10478639

Corcho Alvarado, J. A., Barbecot, F., Purtschert, R., Gillon, M., Aeschbach-Hertig, W., & Kipfer, R. (2009). European climate variations over the past half-millennium reconstructed from groundwater. *Geophysical Research Letters*, *36*(15). https://doi.org/10.1029/2009gl038826

Corcho Alvarado, J. A., Purtschert, R., Barbecot, F., Chabault, C., Rueedi, J., Schneider, V., Aeschbach-Hertig, W. et al. (2007). Constraining the age distribution of highly mixed groundwater using 39Ar: A multiple environmental tracer (^{3}H/^{3}He, 85Kr, 39Ar, and 14C) study in the semiconfined Fontainebleau Sands Aquifer (France). *Water Resources Research*, *43*(3), W03427. https://doi.org/10.1029/2006wr005096

de Jong, M., Moran, J. E., & Visser, A. (2020). Identifying paleowater in California drinking water wells. *Quaternary International*, *547*, 197–207. https://doi.org/10.1016/j.quaint.2019.04.008

Delsman, J. R., Hu-A-Ng, K. R. M., Vos, P. C., De Louw, P. G., Oude Essink, G. H., Stuyfzand, P. J., & Bierkens, M. F. (2014). Paleo-modeling of coastal saltwater intrusion during the Holocene: An application to the Netherlands. *Hydrology and Earth System Sciences*, *18*(10), 3891–3905. https://doi.org/10.5194/hess-18-3891-2014

Duffy, C. J., & Lee, D.-H. (1992). Base flow response from nonpoint source contamination: Simulated spatial variability in source, structure, and initial condition. *Water Resources Research*, *28*(3), 905. https://doi.org/10.1029/91wr02646

Eberts, S. M., Böhlke, J. K., Kauffman, L. J., & Jurgens, B. C. (2012). Comparison of particle-tracking and lumped-parameter age-distribution models for evaluating vulnerability of production wells to contamination. *Hydrogeology Journal*, *20*(2), 263–282. https://doi.org/10.1007/s10040-011-0810-6

Etcheverry, D., & Perrochet, P. (2000). Direct simulation of groundwater transit-time distributions using the reservoir theory. *Hydrogeology Journal*, *8*(2), 200–208. https://doi.org/10.1007/s100400050006

EU. (2006). *Directive 2006/118/EC of the European Parliament and of the Council of 12 December 2006 on the protection of groundwater against pollution and deterioration*. (Vol. 372, pp. 19–31). Official Journal of the European Union.

Gardner, W. P., Harrington, G. A., Solomon, D. K., & Cook, P. G. (2011). Using terrigenic 4He to identify and quantify regional groundwater discharge to streams. *Water Resources Research*, *47*(6), W06523. https://doi.org/10.1029/2010wr010276

Geluk, M. C., Duin, E. T., Dusar, M., Rijkers, R. H. B., Van den Berg, M. W., & Van Rooijen, P. (1995). Stratigraphy and tectonics of the Roer Valley Graben. *Geologie en Mijnbouw*, *73*, 129.

Glasbergen, P. (1987). Hydrological model studies and natural isotope data as indication for groundwater flow in deep sedimentary basins. In *Natural analogs in radioactive waste disposal* (pp. 420–435). Springer Netherlands. https://doi.org/10.1007/978-94-009-3465-8_36

Glasbergen, P., & Mook, W. G. (1982). Natuurlijke isotopen als een hulpmiddel bij regionaal geohydrologisch onderzoek in de provincie Groningen. *H2O*, *26*, 682–704.

Gleeson, T., Wada, Y., Bierkens, M. F. P., & van Beek, L. P. H. (2012). Water balance of global aquifers revealed by groundwater footprint. *Nature*, *488*, 7410:197. https://doi.org/10.1038/nature11295

Goode, D. J. (1996). Direct simulation of groundwater age. *Water Resources Research*, *32*(2), 289–296. https://doi.org/10.1029/95wr03401

Green, C. T., Böhlke, J. K., Bekins, B. A., & Phillips, S. P. (2010). Mixing effects on apparent reaction rates and isotope fractionation during denitrification in a heterogeneous aquifer. *Water Resources Research*, *46*(8), W08525. https://doi.org/10.1029/2009wr008903

Griffioen, J., Vermooten, S., & Janssen, G. (2013). Geochemical and palaeohydrological controls on the composition of shallow groundwater in the Netherlands. *Applied Geochemistry*, *39*, 129–149. https://doi.org/10.1016/j.apgeochem.2013.10.005

Grift, B., van der, G., Janssen, G., Verkaik, J., & Hendriks, D. (2012). Netherlands hydrologic instrument: Water quality modeling, interaction groundwater-surface water. Deltares report 1205735-000.

Han, L. F., & Plummer, L. N. (2016). A review of single-sample-based models and other approaches for radiocarbon dating of dissolved inorganic carbon in groundwater. *Earth-Science Reviews*, *152*, 119–142. https://doi.org/10.1016/j.earscirev.2015.11.004

Hansen, B., Thorling, L., Dalgaard, T., & Erlandsen, M. (2010). Trend reversal of nitrate in Danish groundwater-A reflection of agricultural practices and nitrogen surpluses since 1950. *Environmental Science & Technology*, *45*(1), 228–234.

Hijma, M. P., Cohen, K. M., Roebroeks, W., Westerhoff, W. E., & Busschers, F. S. (2012). Pleistocene Rhine–Thames landscapes: Geological background for hominin occupation of the southern North Sea region. *Journal of Quaternary Science*, *27*(1), 17–39. https://doi.org/10.1002/jqs.1549

Hilton, D. R. (2007). The leaking mantle. *Science*, *318*(5855), 1389–1390. https://doi.org/10.1126/science.1151983

Hinsby, K., Højberg, A. L., Engesgaard, P., Jensen, K. H., Larsen, F., Plummer, L. N., & Busenberg, E. (2007). Transport and degradation of chlorofluorocarbons (CFCs) in the pyritic Rabis Creek aquifer, Denmark. *Water Resources Research*, *43*, W10423. https://doi.org/10.1029/2006wr005854

Houben, G. J., Koeniger, P., & Sültenfuß, J. (2014). Freshwater lenses as archive of climate, groundwater recharge, and hydrochemical evolution: Insights from depth-specific water isotope analysis and age determination on the island of L angeoog, Germany. *Water Resources Research*, *50*(10), 8227–8239. https://doi.org/10.1002/2014wr015584

Houtgast, R. F., & Van Balen, R. T. (2000). Neotectonics of the Roer Valley rift system, the Netherlands. *Global and Planetary Change*, *27*(1–4), 131–146. https://doi.org/10.1016/s0921-8181(01)00063-7

IAEA/WMO (2018). *Global Network of Isotopes in Precipitation, The GNIP Database*, (last access: November 2018), available at: http://www.iaea.org/water

Ingram, R. G., Hiscock, K. M., & Dennis, P. F. (2007). Noble gas excess air applied to distinguish groundwater recharge conditions. *Environmental Science and Technology*, *41*(6), 1949–1955. https://doi.org/10.1021/es061115r

Isarin, R. F., Renssen, H., & Vandenberghe, J. (1998). The impact of the North Atlantic Ocean on the Younger Dryas climate in northwestern and central Europe. *Journal of Quaternary Science: Published for the Quaternary Research Association*, *13*(5), 447–453. https://doi.org/10.1002/(sici)1099-1417(1998090)13:5<447::aid-jqs402>3.0.co;2-b

Jacobs, A. F., Heusinkveld, B. G., & Holtslag, A. A. (2011). Long-term record and analysis of soil temperatures and soil heat fluxes in a grassland area, The Netherlands. *Agricultural and Forest Meteorology*, *151*(7), 774–780. https://doi.org/10.1016/j.agrformet.2011.01.002

Jasechko, S. (2016). Late-Pleistocene precipitation δ18O interpolated across the global landmass. *Geochemistry, Geophysics, Geosystems*, *17*, 3274–3288. https://doi.org/10.1002/2016GC006400

Jasechko, S. (2019). Global Isotope Hydrogeology—Review. *Reviews of Geophysics*, *57*, 835–965. https://doi.org/10.1029/2018RG000627

Jenkins, W. J., Lott, D. E., & Cahill, K. L. (2019). A determination of atmospheric helium, neon, argon, krypton, and xenon solubility concentrations in water and seawater. *Marine Chemistry*, *211*, 94–107. https://doi.org/10.1016/j.marchem.2019.03.007

Jung, M., & Aeschbach, W. (2018). A new software tool for the analysis of noble gas data sets from (ground) water. *Environmental Modelling & Software*, *103*, 120–130. https://doi.org/10.1016/j.envsoft.2018.02.004

Jung, M., Wieser, M., von Oehsen, A., & Aeschbach-Hertig, W. (2013). Properties of the closed-system equilibration model for dissolved noble gases in groundwater. *Chemical Geology*, *339*, 291–300. https://doi.org/10.1016/j.chemgeo.2012.08.006

Jurgens, B. C., Böhlke, J. K., Kauffman, L. J., Belitz, K., & Esser, B. K. (2016). A partial exponential lumped parameter model to evaluate groundwater age distributions and nitrate trends in long-screened wells. *Journal of Hydrology*, *543*, 109–126. https://doi.org/10.1016/j.jhydrol.2016.05.011

Jurgens, B. C., et al. (2012). TracerLPM (Version 1): An Excel® workbook for interpreting groundwater age distributions from environmental tracer data: U.S. Geological Survey Techniques and Methods Report 4-F3, 60 pp, U.S. Geological Survey, Reston, Virginia.

Kaandorp, V. P., De Louw, P. G. B., vander Velde, Y., & Broers, H. P. (2018). Transient groundwater travel time distributions and age-ranked storage-discharge relationships of three lowland catchments. *Water Resources Research*, *54*(7), 4519–4536. https://doi.org/10.1029/2017wr022461

Kasse, C. (1988). Early-Pleistocene tidal and fluviatile environments in the southern Netherlands and northern Belgium. PhD 1090 Thesis Vrije Universiteit Amsterdam. Free University Press.

Klump, S., Grundl, T., Purtschert, R., & Kipfer, R. (2008). Groundwater and climate dynamics derived from noble gas, 14C, and stable isotope data. *Geology*, *36*(5), 395–398. https://doi.org/10.1130/g24604a.1

KNMI. (2012). Climate Atlas Long-term averages 1981-2010 (accessible online: http://www.klimaatatlas.nl/), edited, KNMI, De 1094 Bilt.

Kralik, M., Humer, F., Fank, J., Harum, T., Klammler, G., Gooddy, D., et al. (2014). Using 18O/2H, 3H/3He, 85Kr and CFCs to determine mean residence times and water origin in the Grazer and Leibnitzer Feld groundwater bodies (Austria). *Applied Geochemistry*, *50*, 150–163. https://doi.org/10.1016/j.apgeochem.2014.04.001

Kulongoski, J. T., Hilton, D. R., & Izbicki, J. A. (2005). Source and movement of helium in the eastern Morongo groundwater Basin: The influence of regional tectonics on crustal and mantle helium fluxes. *Geochimica et Cosmochimica Acta*, *69*(15), 3857–3872. https://doi.org/10.1016/j.gca.2005.03.001

Laier, T. (2014). Nitrate monitoring and CFC-age dating of shallow groundwaters—An attempt to check the effect of restricted use of fertilisers. In. *Nitrates in groundwater* (pp. 263–274). CRC Press.

Landon, M. K., Green, C. T., Belitz, K., Singleton, M. J., Esser, B. K. (2011). Relations of hydrogeologic factors, groundwater reduction-oxidation conditions, and temporal and spatial distributions of nitrate, Central-Eastside San Joaquin Valley, California, USA. *Hydrogeology Journal*, *19*(6), 1203–1224. https://doi.org/10.1007/s10040-011-0750-1

Lapperre, R. E., Kasse, C., Bense, V. F., Woolderink, H. A., & Van Balen, R. T. (2019). An overview of fault zone permeabilities and groundwater level steps in the Roer Valley Rift System. *Netherlands Journal of Geosciences*, *98*. https://doi.org/10.1017/njg.2019.4

Leenders, K. A. H. W. (1989). *Verdwenen venen: Een onderzoek naar de ligging en exploitatie van thans verdwenen venen in het gebied tussen Antwerpen, Turnhout, Geertruidenberg en Willemstad (1250-1750)*. Pudoc.

Leenders, K. A. H. W. (1996). Van Turnhoutervoorde tot Strienmonde. Ontginnings-en nederzettingsgeschiedenis van het noordwesten van het Maas-Schelde-Demergebied (400-1350): Een poging tot een synthese. PhD Thesis Universiteit van Amsterdam. Zutphen Walburg Pers (ISBN: 9060119703).

Leray, S., Engdahl, N. B., Massoudieh, A., Bresciani, E., & McCallum, J. (2016). Residence time distributions for hydrologic systems: Mechanistic foundations and steady-state analytical solutions. *Journal of Hydrology*, *543*, 67–87. https://doi.org/10.1016/j.jhydrol.2016.01.068

Loosli, H. H. (1983). A dating method with 39Ar. *Earth and Planetary Science Letters*, *63*(1), 51–62. https://doi.org/10.1016/0012-821x(83)90021-3

Luijendijk, E. (2012). The role of fluid flow in the thermal history of sedimentary basins: Inferences from thermochronology and numerical modeling in the Roer Valley Graben, southern Netherlands. PhD Thesis,Vrije Universiteit, Amsterdam. isbn 9789462030381″. NSG Publication 20120521.

Luijendijk, E., ter Voorde, M., van Balen, R., Verweij, H., & Simmelink, E. (2011). Thermal state of the Roer Valley Graben, part of the European cenozoic rift system. *Basin Research*, *23*(1), 65–82. https://doi.org/10.1111/j.1365-2117.2010.00466.x

Luijendijk, E., Van Balen, R. T., Ter Voorde, M., & Andriessen, P. A. M. (2011). Reconstructing the Late Cretaceous inversion of the Roer Valley Graben (southern Netherlands) using a new model that integrates burial and provenance history with fission track thermochronology. *Journal of Geophysical Research*, *116*(B06402), 1–19. https://doi.org/10.1029/2010jb008071

Maloszewski, P., & Zuber, A. (1982). Determining the turnover time of groundwater systems with the aid of environmental tracers. 1. Models and their applicability. *Journal of Hydrology*, *57*(3–4), 207–231.

Maloszewski, P., & Zuber, A. (1993). Principles and practice of calibration and validation of mathematical models for the interpretation of environmental tracer data in aquifers. *Advances in Water Resources*, *16*(3), 173. https://doi.org/10.1016/0309-1708(93)90036-f

Maloszewski, P., & Zuber, A. (1998). A general lumped parameter model for the interpretation of tracer data and transit time calculation in hydrologic systems - Comments. *Journal of Hydrology*, *204*(1–4), 297–300.

Manning, A. H., Solomon, D.K., Thiros, S.A. (2005). H-3/He-3 age data in assessing the susceptibility of wells to contamination. *Ground Water*, *43*(3), 353–367. https://doi.org/10.1111/j.1745-6584.2005.0028.x

Marcott, S. A., Shakun, J. D., Clark, P. U., & Mix, A. C. (2013). A reconstruction of regional and global temperature for the past 11,300 years. *Science*, *339*(6124), 1198–1201. https://doi.org/10.1126/science.1228026

Massmann, G., Sültenfuß, J., & Pekdeger, A. (2009). Analysis of long-term dispersion in a river-recharged aquifer using tritium/helium data. *Water Resources Research*, *45*, W02431. https://doi.org/10.1029/2007WR006746

Massoudieh, A., Visser, A., Sharifi, S., & Broers, H. P. (2014). A Bayesian modeling approach for estimation of a shape-free groundwater age distribution using multiple tracers. *Applied Geochemistry*, *50*, 252–264. https://doi.org/10.1016/j.apgeochem.2013.10.004

McCallum, J. L., Cook, P. G., Dogramaci, S., Purtschert, R., Simmons, C. T., & Burk, L. (2017). Identifying modern and historic recharge events from tracer-derived groundwater age distributions. *Water Resources Research*, *53*(2), 1039–1056. https://doi.org/10.1002/2016wr019839

Meinardi, C. R. (1994). Groundwater recharge and travel times in the sandy regions of the Netherlands. PhD Thesis VU Amsterdam. RIVM report no. 715501004.

Mendizabal, I., Baggelaar, P. K., & Stuyfzand, P. J. (2012). Hydrochemical trends for public supply well fields in The Netherlands (1898–2008), natural backgrounds and upscaling to groundwater bodies. *Journal of Hydrology*, *450*, 279–292. https://doi.org/10.1016/j.jhydrol.2012.04.050

Mendizabal, I., & Stuyfzand, P. J. (2011). Quantifying the vulnerability of well fields towards anthropogenic pollution: The Netherlands as an example. *Journal of Hydrology*, *398*, 260–276. https://doi.org/10.1016/j.jhydrol.2010.12.026

Mook, W. G. (2006). *Introduction to isotope hydrology*. Taylor and Francis.

Negele, S. (2020). *Enhancing noble gas data evaluation based on high precision solubilities from literature*. [Master thesis, Heidelberg University].

Nolan, B. T., Ruddy, B. C., Hitt, K. J., Helsel, D. R. (1997). Risk of nitrate in groundwaters of the United States - A national perspective. *Environmental Science and Technology*, *31*(8), 2229. https://doi.org/10.1021/es960818d

Oeschger, H., Gugelmann, A., Loosli, H., Schotterer, U., Siegenthaler, U., & Wiest, W. (1974). 39Ar dating of groundwater, in Isotope Techniques in Groundwater Hydrology, edited, pp. 179-190, International Atomic Energy Agency, Vienna.

Osenbrück, K., Fiedler, S., Knöller, K., Weise, S. M., Sültenfuß, J., Oster, H., & Strauch, G. (2006). Timescales and development of groundwater pollution by nitrate in drinking water wells of the Jahna-Aue, Saxonia, Germany. *Water Resources Research*, *42*(12), W12416. https://doi.org/10.1029/2006wr004977

Pétré, M. A., Rivera, A., Lefebvre, R., Hendry, M. J., & Folnagy, A. J. (2016). A unified hydrogeological conceptual model of the Milk River transboundary aquifer, traversing Alberta (Canada) and Montana (USA). *Hydrogeology Journal*, *24*(7), 1847–1871. https://doi.org/10.1007/s10040-016-1433-8

Plummer, L. N., Busenberg, E., Böhlke, J. K., Nelms, D. L., Michel, R. L. & Schlosser, P. (2001). Groundwater residence times in Shenandoah National Park, Blue Ridge Mountains, Virginia, USA: A multi-tracer approach. *Chemical Geology*, *179*(1–4), 93–111. https://doi.org/10.1016/s0009-2541(01)00317-5

Poreda, R. J., Cerling, T. E. & Salmon, D. K. (1988). Tritium and Helium-Isotopes as Hydrologic Tracers in a Shallow Unconfined Aquifer. *Journal of Hydrology*, *103*(1–2), 1–9. https://doi.org/10.1016/0022-1694(88)90002-9

Renssen, H., Kasse, C., Vandenberghe, J., & Lorenz, S. J. (2007). Weichselian Late Pleniglacial surface winds over northwest and central Europe: A model–data comparison. *Journal of Quaternary Science*, *22*(3), 281–293. https://doi.org/10.1002/jqs.1038

Schilling, K. E., Anderson, R., Alexander, C., Peate, D., & Dorale, J. (2015). Mining unique soft and old water within the Manson Impact Structure. *Hydrogeology Journal*, *23*, 95–103. https://doi.org/10.1007/s10040-014-1193-2

Schlosser, P., Dörr, H., Sonntag, H., Münnich, K. O. (1988). Tritium/3He Dating of Shallow Groundwater. *Earth and Planetary Science Letters*, *89*(3–4), 353–362. https://doi.org/10.1016/0012-821x(88)90122-7

Sebol, L. A., et al. (2007). Evidence of CFC degradation in groundwater under pyrite-oxidizing conditions. *Journal of Hydrology*, *347*(1–2), 1–12. https://doi.org/10.1016/j.jhydrol.2007.08.009

Solomon, D. K., Robertson, W. D., Busenberg, E., Plummer, L. N., Ryan, M. C. & Schiff, S. L. (1996). Source of radiogenic helium 4 in shallow aquifers: Implications for dating young groundwater. *Water Resources Research*, *32*(6), 1805–1813. https://doi.org/10.1029/96wr00600

Stute, M., & Deak, J. (1989). Environmental isotope study (14 C, 13 C, 18 O, D, noble gases) on deep groundwater circulation systems in Hungary with reference to paleoclimate. *Radiocarbon*, *31*(3), 902–918. https://doi.org/10.1017/s0033822200012522

Stuurman, R. J., Van der Meij, J. L., Engelen, G. B., Biesheuvel, A., & van Zadelhoff, E. (1989). Hydrological system analysis of the greater Noord-Brabant region. Final report: an integral investigation on the structure and dynamics of groundwater systems and associated threats. TNO-DGV, report OS, 90–25A (In Dutch).

Stuurman, R. J., Witte, J. P. M., vander Meijden, R., & Groen, C. L. G. (1996). National Hydrological Systems Analysis. Report 5. Regional Groundwater Flow Systems of the Campian Plateau, the Brabant cover sand ridges and the Limburg Meuse Terraces. Report TNO Groundwater and Geo_Energy GG.-R-96-66(B). (In Dutch)

Stuyfzand, P. J. (1993). Hydrochemistry and hydrology of the coastal dune area of the Western Netherlands. PhD Thesis Vrije Universiteit Amsterdam (ISBN: 9074741010).

Suckow, A. (2014). The age of groundwater – Definitions, models and why we do not need this term. *Applied Geochemistry*, *50*, 222–230. https://doi.org/10.1016/j.apgeochem.2014.04.016

Sukhija, B. S., Reddy, D. V., & Nagabhushanam, P. (1998). Isotopic fingerprints of paleoclimates during the last 30,000 years in deep confined groundwaters of Southern India. *Quaternary Research*, *50*(3), 252–260. https://doi.org/10.1006/qres.1998.2001

Sültenfuß, J., Purtschert, R., & Jens, F. (2011). Age structure and recharge conditions of a coastal aquifer (northern Germany) investigated with ^{39}Ar, ^{14}C, ^{3}H, He isotopes and Ne. *Hydrogeology Journal*, *19*(1), 221–236. https://doi.org/10.1007/s10040-010-0663-4

Sültenfuß, J., Roether, W., & Rhein, M. (2009). The Bremen mass spectrometric facility for the measurement of helium isotopes, neon, and tritium in water. *Isotopes in Environmental and Health Studies*, *45*(2), 83–95. https://doi.org/10.1080/10256010902871929

Sun, T., Hall, C. M., & Castro, M. C. (2010). Statistical properties of groundwater noble gas paleoclimate models: Are they robust and unbiased estimators? *Geochemistry, Geophysics, Geosystems*, *11*, Q02003. https://doi.org/10.1029/2009GC002717

TNO-GSN (2021). Wouw Member. In.*Stratigraphic nomenclature of the Netherlands, TNO – geological survey of the Netherlands*. Accessed on 11-06-2021 from http://www.dinoloket.nl/en/stratigraphic-nomenclature/wouw-member

Vandenberghe, J., Coope, R., & Kasse, K. (1998). Quantitative reconstructions of palaeoclimates during the last interglacial–glacial in western and central Europe: An introduction. *Journal of Quaternary Science: Published for the Quaternary Research Association*, *13*(5), 361–366. https://doi.org/10.1002/(sici)1099-1417(1998090)13:5<361::aid-jqs404>3.0.co;2-o

Vandenberghe, J., Lowe, J., Coope, R., Litt, T., & Züller, L. (2004). Climatic and environmental variability in the mid-latitude Europe sector during the last interglacial-glacial cycle. In *Past climate variability through Europe and Africa* (pp. 393–416). Springer.

Van Wees, J. D., Buijze, L., Van Thienen-Visser, K., Nepveu, M., Wassing, B. B. T., Orlic, B. (2014). Geomechanics response and induced seismicity during gas field depletion in the Netherlands. *Geothermics*, *52*, 206–219. https://doi.org/10.1016/j.geothermics.2014.05.004

Varsányi, I., Palcsu, L., & Kovács, L. Ó. (2011). Groundwater flow system as an archive of paleotemperature: Noble gas, radiocarbon, stable isotope and geochemical study in the Pannonian Basin, Hungary. *Applied Geochemistry*, *26*(1), 91–104. https://doi.org/10.1016/j.apgeochem.2010.11.006

Verbeek, J. W., De Leeuw, C. S., Parker, N., & Wong, T. E. (2002). Characterization and correlation of Tertiary seismostratigraphic units in the Roer Valley Graben. *Netherlands Journal of Geosciences*, *81*(2), 159–166. https://doi.org/10.1017/s0016774600022393

Visser, A., Broers, H.P., Heerdink, R., & Bierkens, M.F.P. (2009). Trends in pollutant concentrations in relation to time of recharge and reactive transport at the groundwater body scale. *Journal of Hydrology*(3–4), 427–439. https://doi.org/10.1016/j.jhydrol.2009.02.008

Visser, A., Broers, H. P., Purtschert, R., Sültenfuß, J., & de Jonge, M. (2013). Groundwater age distributions at a public drinking water supply well field derived from multiple age tracers (85Kr, 3H/3He, and 39Ar). *Water Resources Research*, *49*(11), 7778–7796. https://doi.org/10.1002/2013wr014012

Visser, A., Broers, H. P., Van der Grift, B., & Bierkens, M. F. P. (2007). Demonstrating trend reversal of groundwater quality in relation to time of recharge determined by 3H/3He. *Environmental Pollution*, *148*(3), 797–807. https://doi.org/10.1016/j.envpol.2007.01.027

Visser, A., Dubus, I. G., Broers, H. P., Brouyere, S., Korcz, M., Orban, Ph., et al. (2009). Comparison of methods for the detection and extrapolation of trends in groundwater quality. *Journal of Environmental Monitoring*, *11*(11), 2030. https://doi.org/10.1039/b905926a

Visser, A., Schaap, J. D., Broers, H. P., & Bierkens, M. F. P. (2009). Degassing of $^{3}H/^{3}He$, CFCs and SF6 by denitrification: Measurements and two-phase transport simulations. *Journal of Contaminant Hydrology*, *103*(3–4), 206–218. https://doi.org/10.1016/j.jconhyd.2008.10.013

Vogel, J. C. (1967).Investigation of groundwater flow with radiocarbon. , paper presented at IAEA Symposium on Isotopes in Hydrology, 14-18 November 1966, IAEA, Vienna, Austria.

Vos, P. (2015). Origin of the Dutch coastal landscape: long-term landscape evolution of the Netherlands during the Holocene, described and visualized in national, regional and local palaeogeographical map series. PhD Thesis Utrecht University. Barkhuis, ISBN 9789491431821.

Wei, W., Aeschbach-Hertig, W., & Chen, Z. (2015). Identification of He sources and estimation of He ages in groundwater of the North China Plain. *Applied Geochemistry*, *63*, 182–189. https://doi.org/10.1016/j.apgeochem.2015.08.010

Yu, L., Rozemeijer, J., Van Breukelen, B. M., Ouboter, M., Van Der Vlugt, C., & Broers, H. P. (2018). Groundwater impacts on surface water quality and nutrient loads in lowland polder catchments: Monitoring the greater Amsterdam area. *Hydrology and Earth System Sciences*, *22*(1). https://doi.org/10.5194/hess-22-487-2018

Zhang, Y. C., Slomp, C. P., Broers, H. P., Bostick, B., Passier, H. F., Böttcher, M. E., et al. (2012). Isotopic and microbiological signatures of pyrite-driven denitrification in a sandy aquifer. *Chemical Geology*, *300*, 123–132. https://doi.org/10.1016/j.chemgeo.2012.01.024

Zhang, Y.-C., Slomp, C. P., Broers, H. P., Passier, H. F., Cappellen, P. V. (2009). Denitrification coupled to pyrite oxidation and changes in groundwater quality in a shallow sandy aquifer. *Geochimica et Cosmochimica Acta*, *73*(22), 6716–6726. https://doi.org/10.1016/j.gca.2009.08.026

Zinn, B. A., & Konikow, L. F. (2007). Potential effects of regional pumpage on groundwater age distribution. *Water Resources Research*, *43*(6). https://doi.org/10.1029/2006wr004865

References From the Supporting Information

Aravena, R., Wassenaar, L. I., & Plummer, L. N. (1995). Estimating 14C groundwater ages in a methanogenic aquifer. *Water Resources Research*, *31*(9), 2307–2317.

Bakker, I., Kiden, P., Schokker, J., & Griffioen, J. (2007). *De geotop van de ondergrond: Een reactievat. Deelrapport 2. Eerste statistische karakterisatie van de geochemische reactiecapaciteit van het topsysteem in Noord-Brabant en het noorden van Limburg* (Report No. 2007-UR0324/A). TNO Bouw en Ondergrond

Barker, J. F., Fritz, P., & Brown, R. M. (1979). Carbon-14 measurements in aquifers with methane. *Isotope hydrology 1978*.

Eichinger, L. (1983). A contribution to the interpretation of 14 C groundwater ages considering the example of a partially confined sandstone aquifer. *Radiocarbon*, *25*(2), 347–356.

Friedrich, R. (2007). *Environmental tracers for groundwater studies: Investigation of groundwater in the Odenwald region and implementation of a new noble gas mass-spectrometric system*. Thesis University of Heidelberg.

Griffioen, J., Klaver, G., & Westerhoff, W. E. (2016). The mineralogy of suspended matter, fresh and Cenozoic sediments in the fluvio-deltaic Rhine–Meuse–Scheldt–Ems area, the Netherlands: An overview and review. *Netherlands Journal of Geosciences - Geologie en Mijnbouw*, *95*(1), 23–107. https://doi.org/10.1017/njg.2015.32

Han, L. F., & Plummer, L. N. (2013). Revision of Fontes and Garnier's model for the initial 14C content of dissolved inorganic carbon used in groundwater dating. *Chemical Geology*, *351*, 105–114.

Sültenfuß, J., Roether, W., & Rhein, M. (2009). The Bremen mass spectrometric facility for the measurement of helium isotopes, neon, and tritium in water. *Isotopes in Environmental and Health Studies*, *45*(2), 83–95. https://doi.org/10.1080/10256010902871929

Tamers, M. A. (1967). Radiocarbon ages of groundwater in an arid zone unconfined aquifer. *Isotope techniques in the hydrologic cycle*, *11*, 143–152.

Wijma, S., Aerts, A. T., vanderPlicht, J., & ZondervanJun, A. (1996). Nuclear Instruments and Methods in Physics Research Section B-Beam Interactions with Materials and Atoms (Vol. 113, pp. 465–469).